Accepted Manuscript

Are the Dorsa Argentea on Mars eskers?
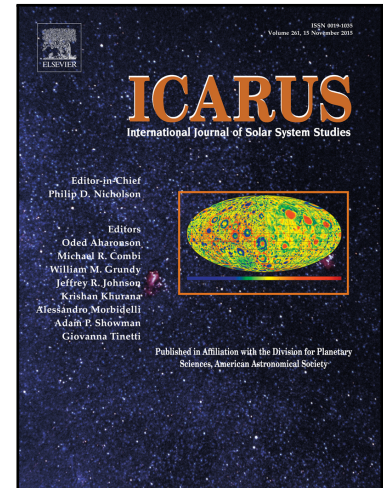
Frances E.G. Butcher , Susan J. Conway , Neil S. Arnold

Please cite this article as: Frances E.G. Butcher , Susan J. Conway , Neil S. Arnold , Are the Dorsa Argentea on Mars eskers?, *Icarus* (2016), doi: 10.1016/j.icarus.2016.03.028

Highlights:

- Geometries of the Dorsa Argentea on Mars are statistically similar to >20 000 terrestrial eskers.

- Variations in ridge cross-sectional morphology are consistent with terrestrial eskers.

- Statistical tests confirm esker-like relationships between ridge height and bed slope.

- The ridges may have formed in subglacial conduits terminating in a proglacial lake.

- Quantitative characterisations may be useful for modelling putative former ice sheet hydrology.

Are the Dorsa Argentea on Mars eskers?

Frances E.G. Butcher[1]*, Susan J. Conway[1,2], Neil S. Arnold[3]

[1] Department of Physical Sciences, The Open University, Walton Hall, Milton Keynes, MK7 6AA, United Kingdom. Email: frances.butcher@open.ac.uk

[2] Laboratoire de Planétologie et Géodynamique de Nantes - UMR CNRS 6112, 2 rue de la Houssinière - BP 92208, 44322 Nantes Cedex 3, France.

[3] Scott Polar Research Institute, University of Cambridge, Lensfield Road, Cambridge, CB2 1ER, United Kingdom.

*Corresponding author

Abstract

The Dorsa Argentea are an extensive assemblage of ridges in the southern high latitudes of Mars. They have previously been interpreted as eskers formed by deposition of sediment in subglacial meltwater conduits, implying a formerly more extensive south polar ice sheet. In this study, we undertake the first large-scale statistical analysis of aspects of the geometry and morphology of the Dorsa Argentea in comparison with terrestrial eskers in order to evaluate this hypothesis. The ridges are re-mapped using integrated topographic (MOLA) and image (CTX/HRSC) data, and their planar geometries compared to recent characterisations of terrestrial eskers. Quantitative tests for esker-like relationships between ridge height, crest morphology and topography are then completed for four major Dorsa Argentea ridges. The following key conclusions are reached: (1) Statistical distributions of lengths and sinuosities of the Dorsa Argentea are similar to those of terrestrial eskers in

Canada. (2) Planar geometries across the Dorsa Argentea support formation of ridges in conduits extending towards the interior of an ice sheet that thinned towards its northern margin, perhaps terminating in a proglacial lake. (3) Variations in ridge crest morphology are consistent with observations of terrestrial eskers. (4) Statistical tests of previously observed relationships between ridge height and longitudinal bed slope, similar to those explained by the physics of meltwater flow through subglacial meltwater conduits for terrestrial eskers, confirm the strength of these relationships for three of four major Dorsa Argentea ridges. (5) The new quantitative characterisations of the Dorsa Argentea may provide useful constraints for parameters in modelling studies of a putative former ice sheet in the south polar regions of Mars, its hydrology, and mechanisms that drove its eventual retreat.

1. Introduction

The Dorsa Argentea are an assemblage of ~7000 kilometres of ridges in the southern high latitudes of Mars (70° - 80°S, 56°W - 6°E). They give their name to the Dorsa Argentea Formation (DAF, equivalent to the Hesperian polar unit in Tanaka et al. (2014a) in which they are located (Fig. 1). The Dorsa Argentea are the most extensive of seven assemblages of ridges distributed throughout the DAF (Kress and Head, 2015). The DAF is adjacent to the present Amazonian-aged (< 3.2 Ga) (Hartmann, 2005) south polar layered deposits (SPLD), comprising water and carbon dioxide (CO_2) ice deposits (Phillips et al., 2011). The DAF is distributed in two major lobes centred on the ~0°E and ~290°E longitude lines (Ghatan and Head, 2004). The Dorsa Argentea trend SE to NW within the ~290°E DAF lobe which extends to ~65°S, with its northernmost extent reaching ~55°S. Within the most recent United States Geological Survey (USGS) global map of Mars (Tanaka et al., 2014a), the DAF is interpreted as remnants of ice-rich deposits emplaced either by cryovolcanic

iii

flows or atmospheric precipitation and subsequently superposed by a thin, periglacially-modified mantle deposit. The DAF is believed to range in thickness from a lag-deposit veneer over the underlying bedrock in the vicinity of the Dorsa Argentea ridges, to a blanket hundreds of metres thick to the south and east (Ghatan and Head, 2004).

The Dorsa Argentea occur in the headward region of Argentea Planum (Ghatan and Head, 2004), a broad, NW-trending, ~975 km long basin in the DAF that is topographically confined by the surrounding cratered highlands (Tanaka et al., 2014a), and enter a narrower ~40 km wide valley at its head. In the central region of their distribution, the ridges generally trend N-NW, diagonal to the strike of the basin (Fig. 1). Here, they emerge from the deposits, which superpose several ridges to an increasing degree towards the south (Head, 2000a; Head and Pratt, 2001), and descend into the basin, before ascending or tracking along the slopes on its distal side. At the NE margin of Argentea Planum (Fig. 1), several ridges turn east and enter the narrow ~550 km-long East Argentea Planum (Ghatan and Head, 2004). Individual ridges have lengths of up to several hundred kilometres (Metzger, 1992) with heights up to 120 m and widths up to 6 km (Head and Pratt, 2001). They range from stand-alone ridges to bifurcating and braided networks (Howard, 1981; Kargel and Strom, 1992), and exhibit evidence of superposition (Head and Hallet, 2001a). Buffered crater counting by Kress and Head (2015) returns a best-fit age of 3.48 Ga for the Dorsa Argentea ridges, corresponding to the Early Hesperian period of Mars' geological history.
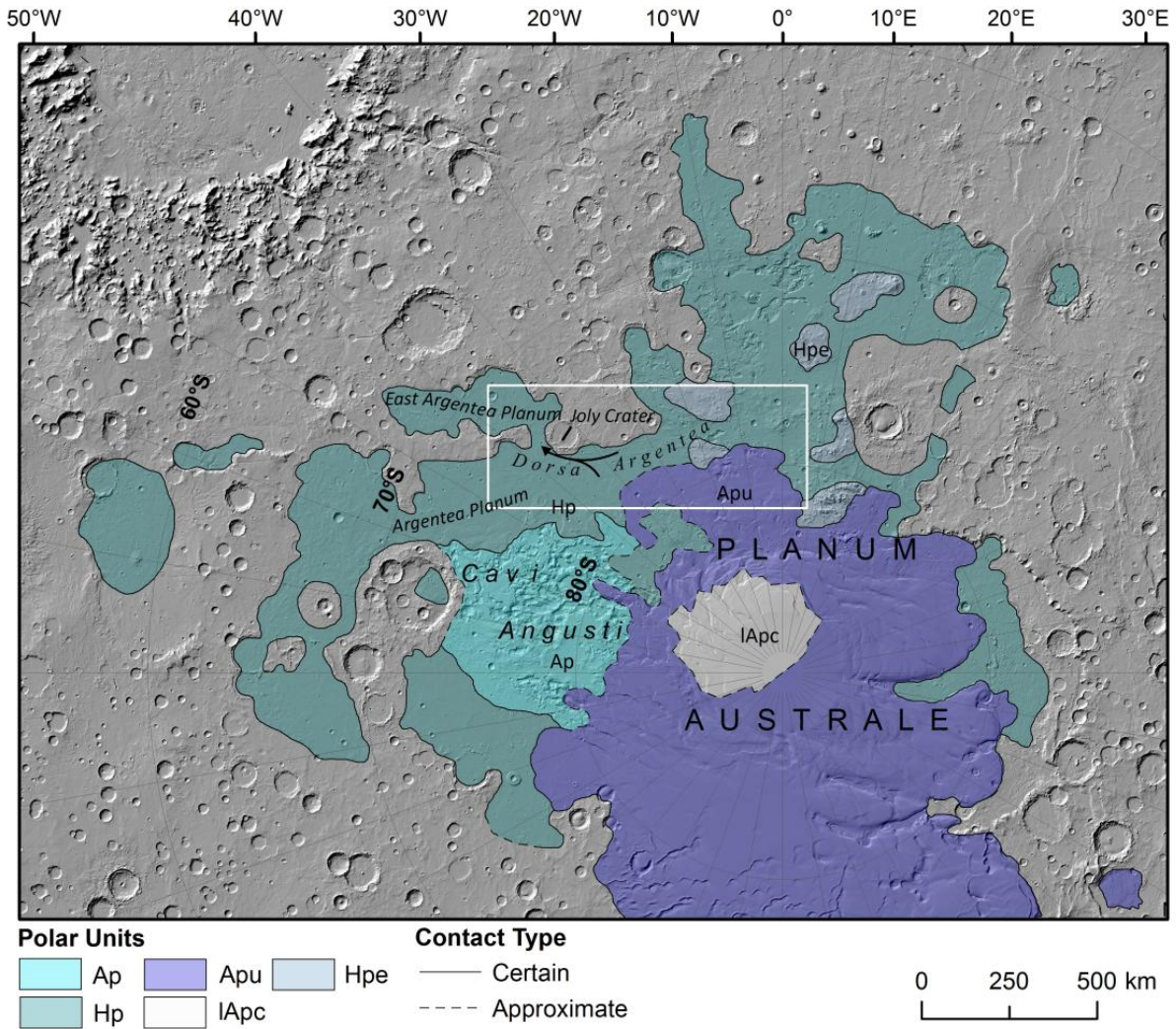
Figure 1: *Map of the south polar region of Mars showing the major surface units* (Tanaka et al., 2014a) *with relevant features labelled, overlain on a hillshade map derived from 460 m/pixel MOLA DEM. The black arrow shows the general trend of the Dorsa Argentea ridges. Ap is the Amazonian polar unit; Apu is the Amazonian polar undivided unit; Hpe is the Hesperian polar edifice unit; Hp is the Hesperian polar unit, equivalent to the Dorsa Argentea Formation (DAF); and IApc is the Late Amazonian polar cap unit. The white box delineates our study area. Projection is south polar stereographic. Surface units, labels and contacts between them are modified from Tanaka et al. (2014a).*

The Dorsa Argentea have previously been interpreted as lacustrine (Parker et al., 1986), volcanic (Tanaka and Scott, 1987; Ruff and Greeley, 1990), tectonic (Kargel, 1993),

3

aeolian (Ruff and Greeley, 1990), erosional (Ruff and Greeley, 1990; Kargel, 1993; Tanaka and Kolb, 2001; Tanaka et al., 2014b) or glaciofluvial features (Howard, 1981; Metzger, 1992; Kargel and Strom, 1992; Kargel, 1993; Head, 2000a, 2000b; Head and Hallet, 2001a, 2001b; Head and Pratt, 2001; Tanaka et al., 2014b; Kress and Head, 2015).

Although many of these interpretations have already been excluded due to morphological inconsistencies with terrestrial analogues (e.g. Head and Pratt, 2001, and references therein), a description of the Dorsa Argentea as either eskers or inverted fluvial channels in the most recent USGS geological map of Mars (Tanaka et al., 2014b) highlights that a consensus on their origin has not yet been reached.

Eskers are ridges formed by deposition of glacial sediment in ice-contact meltwater channels, and subsequent lowering of this material to, or its exposure at, the ground surface during deglaciation (e.g., Banerjee and McDonald, 1975; Brennand, 2000; Benn and Evans, 2010). Complex supraglacial, englacial and subglacial drainage within terrestrial ice sheets gives rise to a diverse range of morphologies and configurations of terrestrial esker systems (e.g., Banerjee and McDonald, 1975; Brennand, 2000; Perkins et al., 2016). Relationships between ridge cross-sectional (CS) dimensions and CS crest morphology and the surrounding topography, similar to those observed for terrestrial eskers, have been identified for the Dorsa Argentea, and explained using Shreve's (1972, 1985a) theory on the physics of meltwater flow through subglacial conduits (Head and Hallet, 2001a, 2001b).

However, no large-scale quantitative tests of these relationships have been presented for the ridges and photogeologic analysis to date has largely been limited to assessment of low-resolution (~150 to 300 m/pixel) images from the Viking Orbiters (e.g., Howard, 1981; Kargel and Strom, 1992; Head, 2000b; Head and Pratt, 2001). Furthermore, no detailed statistical characterisation of planar geometries of a large sample of the Dorsa Argentea ridges has previously been presented, perhaps due to a lack of similarly extensive, ice-sheet-scale datasets for terrestrial esker analogues.

Recent publication of the first large-scale quantitative analysis of planar geometries of terrestrial eskers (Storrar et al., 2014a), formed during deglaciation of the Laurentide Ice

Sheet between 13000 and 7000 years ago (Storrar et al., 2014b), gives a new opportunity for comparison and assessment of the esker hypothesis for the Dorsa Argentea, which we exploit here.

We present extensive quantitative characterisation of planar geometries of the Dorsa Argentea in comparison with the large sample of terrestrial eskers analysed by Storrar et al. (2014a). Additionally, we quantify CS dimensions of four major Dorsa Argentea ridges and classify their crest morphologies using high-resolution topographic (MOLA) and medium-resolution image (CTX) datasets, and present the first statistical assessment of esker-like topographic relationships for the Dorsa Argentea that were previously observed by Head and Hallet (2001a). We therefore present the first rigorous quantitative statistical tests of the hypothesis that the Dorsa Argentea are morphologically consistent with terrestrial eskers. Such assessment is necessary as a growing body of literature uses the interpretation of the Dorsa Argentea as eskers as a basis for inferences about the character of a putative former ice sheet thought to have extended into the DAF during Mars' Hesperian period, and the nature of its recession (Head, 2000a; Head and Pratt, 2001; Milkovich et al., 2002; Ghatan and Head, 2004; Fastook et al., 2012; Scanlon and Head, 2015; Kress and Head, 2015). Similarities have been observed between subparallel curvilinear and isolated linear-curvilinear ridges within ridge assemblages in the Cavi Angusti and Planum Angustum sectors of the DAF, and terminal moraines marking the former extents of terrestrial glaciers and ice sheets (Kress and Head, 2015). If correct, the existence of moraine ridges has implications for the geomorphic record of the former extent and retreat of a putative former ice sheet in the DAF. However, Kress and Head (2015) acknowledge that further investigation of these features is required to test the moraine hypothesis. The quantitative description of the Dorsa Argentea ridges in the present study may provide useful inputs for tests for differences in morphology and, by extension, mechanisms of formation between the Dorsa Argentea and other ridge assemblages in the DAF.

If quantitative and statistical analyses of the Dorsa Argentea and comparison to planar geometries and topographic relationships observed for terrestrial eskers support the

hypothesis that the Dorsa Argentea are eskers, the quantitative characterisations contained within this study may provide useful constraints for parameters in modelling studies of a putative former ice sheet extending into the DAF, its hydrology, and mechanisms that drove its eventual retreat. A lack of sufficient constraints upon the terminus position of this putative ice sheet means that, at present, reconstruction of glacier thickness akin to that performed by Bernhardt et al. (2013) based on ice-surface slopes derived from putative eskers in Argyre Planitia, is not possible for the Dorsa Argentea. Identification of a possible terminus of the putative DAF ice sheet is beyond the scope of the present study, which purely aims to rigorously test the hypothesis that the Dorsa Argentea are eskers.

Furthermore, possible identification of the first martian esker connected to its parent glacier in the Phlegra Montes region (Gallagher and Balme, 2015) suggests that eskers may be widespread geomorphological features diagnostic of glaciated landscapes on Mars (Kargel and Strom, 1992; Banks et al., 2009; Ivanov et al., 2012; Bernhardt et al., 2013; Erkeling et al., 2014). It is therefore necessary to begin a quantitative description of the range of characteristics of putative eskers on Mars to facilitate their identification.

2. Background: Terrestrial eskers

Given the great lengths (>100 km), low degree of fragmentation (Metzger, 1992), location within potential tunnel valleys (Kargel and Strom, 1992), and lack of morainic features associated with the Dorsa Argentea ridges on Mars (Howard, 1981), the terrestrial esker analogues of most interest for the present study are those formed within subglacial conduits beneath a stagnant or sluggish ice mass that does not override sedimentary bedforms during retreat (Metzger, 1991, 1992; Scanlon and Head, 2015; Kress and Head, 2015).

2.1. Planar geometry

6

Eskers adopt the paths of the conduits in which they form, and therefore have similar configurations and geometries to drainage networks formed during deglaciation. Storrar et al. (2014a) present data for the distributions of length, degree of fragmentation and sinuosity of a large sample (n > 20 000) of eskers in Canada. Individual Canadian eskers with lengths up to 97.5 km form longer fragmented chains of eskers up to 760 km in length, in which gaps account for 34.9 % of the total length. Storrar et al. (2014a) attribute these great lengths to time-transgressive formation in spatially and temporally stable meltwater conduits close to the retreating margin of the Laurentide Ice Sheet. However, mechanisms allowing synchronous formation of very long eskers in long, stable conduits extending towards the interior of former ice sheets and terminating in a standing water body have also been described in relation to detailed field studies of Canadian eskers (Brennand, 1994; Brennand and Shaw, 1996; Brennand, 2000). Fragmentation of eskers into shorter segments separated by gaps can be an outcome of changes in sedimentation conditions in subglacial conduits (Shreve, 1972; Banerjee and McDonald, 1975; Brennand, 1994, 2000) and/or post-depositional erosion, including erosion by dynamic ice at a retreating ice margin (Brennand, 2000; Storrar et al., 2014a).

The degree to which eskers diverge from straight paths (sinuosity) may be an outcome of pressure conditions within the subglacial esker-forming conduits (Storrar et al., 2014a). Idealised water-filled meltwater conduits at the base of an ice sheet or glacier, crossing a hard bed, adopt roughly semi-circular cross-sections incised upwards into the overlying ice (R-channels, Röthlisberger, 1972). At the scale of an ice sheet, the direction of subglacial water flow through R-channels is thought to be governed by the subglacial hydraulic potential (Shreve, 1972). At any given point within an ice sheet, the hydraulic potential (ϕ) is a function of the elevation of the point and the water pressure:

$$\phi = \rho_w g z + P_w \tag{1}$$

7

where ρ_w is the density of water, g is gravity, z is the elevation of the point and P_w is the water pressure within the ice. Whilst many factors can influence P_w, a common simplifying assumption (e.g., Flowers, 2015) is that P_w can be assumed to be equal to the pressure of the overlying ice:

$$P_w = \rho_i g(z_s\text{-}z) \tag{2}$$

where ρ_i is the ice density, and z_s is the ice surface elevation. Inserting equation 2 into equation 1, and rearranging gives:

$$\phi = \rho_i g z_s + (\rho_w - \rho_i)gz \tag{3}$$

Given the relative densities of ice and water, equation 3 shows that surfaces of hydraulic equipotential dip up-glacier at ~11 times the ice surface slope (Fig. 2; Shreve, 1972). These surfaces intersect the bed where z equals the bed elevation (Brennand, 2000) to produce contours of equal subglacial potential. Thus, given that meltwater flows along the path of the steepest subglacial hydraulic potential gradient, (i.e. perpendicular to the contours of hydraulic equipotential), the slope of the ice surface is ~11 times as influential as bed topography in determining the path of pressurised water flow in subglacial conduits, and water may ascend topographic features on the bed or track along slopes (Shreve, 1972; Brennand, 2000), provided the bed slope does not exceed 11 times the ice surface slope. This is supported by observations; the ~150 km long terrestrial Katahdin esker system in Maine USA, ascends topographic undulations to reach elevations up to ~100 m above surrounding topographic lows (Shreve, 1985a). On a level bed, eskers track in the direction of the steepest ice surface slope (Shreve, 1972; Brennand, 2000), forming radial patterns away from former ice divides (Storrar et al., 2014a).
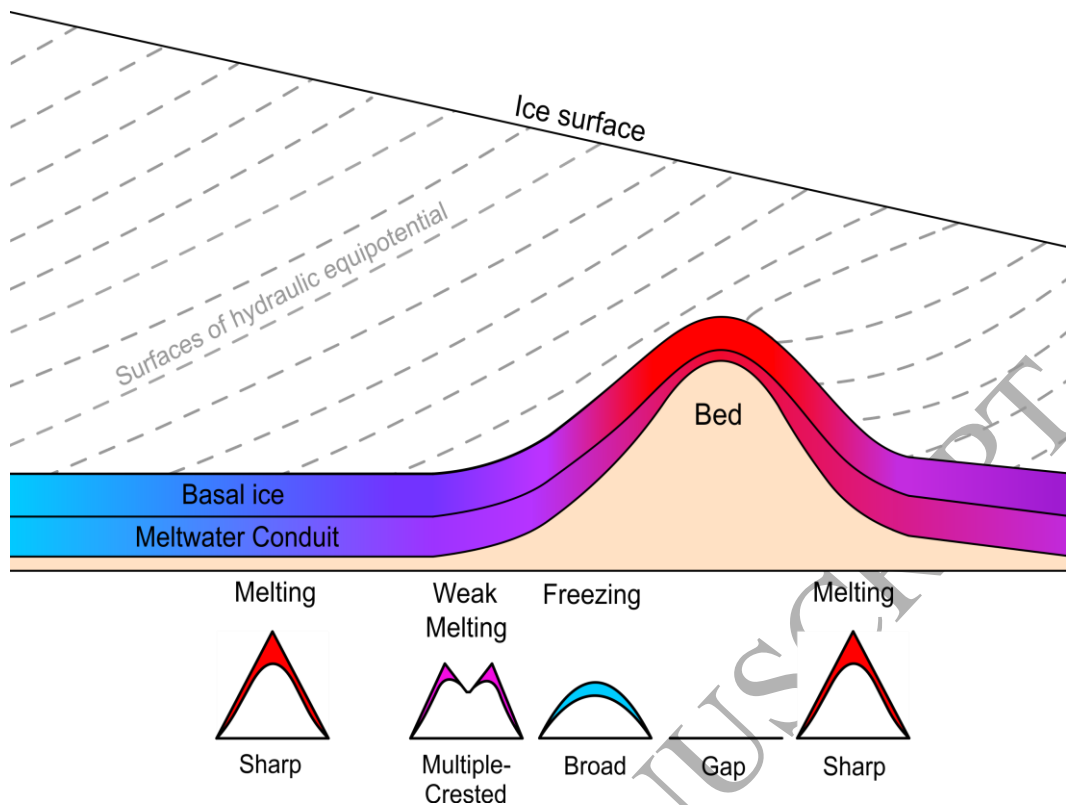
Figure 2: *The relationship between esker crest morphology, dimensions and bed topography described by Shreve (1985a), based on Figure 5 from Shreve (1985a) and Figure 8.64 from Anderson and Anderson (2010). Temperature is represented on a gradient from light blue (cold) through to red (warm). Geometries are not accurate and dimensions are exaggerated for clarity. The reader is referred to the web-version of this article for interpretation of the colours in this figure.*

2.2 Cross-sectional dimensions, crest morphology and relationships to topography

Eskers adopt the CS dimensions and CS crest morphology of subglacial conduits (R-channels; Section 2.1) in which they form, assuming they completely fill the conduits (Banerjee and McDonald, 1975; Shreve, 1985a). Changes in these properties along esker profiles are related the physics of meltwater flow through water-filled R-channels (Fig. 2) (Shreve, 1972, 1985a). This theory was developed based on the terrestrial eskers of the Katahdin esker system in Maine, USA, which have heights of 3-50 m, and typical widths of 150-600 m, but can be up to 2 km-wide (Shreve, 1985a). These dimensions are typical of

most terrestrial eskers (Clark and Walder, 1994), although eskers can have heights and widths of less than 10 m (Storrar et al., 2015).

R-channels are maintained in a steady-state when conduit closure by creep of the surrounding ice is directly opposed by melting of the conduit roof and walls due to viscous heating by meltwater flow (Röthlisberger, 1972). However, changes in ice thickness and associated changes in the pressure melting point (PMP) of ice along conduit paths disrupt steady-state conditions, promoting adjustment of dynamics of conduit wall melting and changes in conduit CS dimensions (Shreve, 1972, 1985a; Anderson and Anderson, 2010). Conduits trend down-glacier into thinner ice with correspondingly higher PMP. Viscous heat produced by frictional interaction of meltwater with the conduit walls must therefore be partitioned towards warming of water to the temperature of the ice into which it passes before opposition of conduit creep closure by wall melting can occur.

On Earth, on a level bed, water warming consumes ~30 % of the available heat energy (Shreve, 1985a) meaning that ~70 % of viscous heat energy is available for wall melting. On descending bed slopes, down-glacier thinning (and warming) of the ice is mediated, promoting stronger wall melting than on a level bed. In contrast, on gently ascending slopes (<~1.7 times the ice surface gradient on Earth) wall melting is weakened as the overlying ice thins downstream more rapidly than over a level bed. On slopes >~1.7 times the ice surface gradient, wall melting transitions into a regime of wall freezing as viscous heating cannot compensate for increases in PMP beneath rapidly thinning ice (Shreve, 1972; Anderson and Anderson, 2010). Changes in the rate of wall melting with bed slope therefore drive changes in the CS dimensions of eskers forming within conduits. The conduit roof experiences greater rates of melting or freezing than the side walls as water in contact with the roof dissipates energy over a smaller surface area relative to its depth (Shreve, 1985a). Therefore, conduit height is more sensitive than width to changes in melt dynamics due to bed topography, resulting in changes in conduit shape (Shreve, 1985a).

Accordingly, as is illustrated in Fig. 2, terrestrial eskers formed on level or gently descending bed slopes may be characterised by tall, sharp crest morphology approximating

10

a triangular shape. In areas ascending <~1.7 times the ice surface slope, weaker roof melting leads to lower, multiple-crested esker crest morphology, and on steeply ascending slopes (>~1.7 times the ice surface slope), eskers adopt a lower, broad-crested morphology (Shreve, 1972, 1985a, 1985b; Anderson and Anderson, 2010).

Depression of surfaces of hydraulic equipotential at the crest of topographic undulations drives local increases in the capacity for sediment transport by meltwater, and may result in gaps between related esker segments forming on either side of a topographic undulation within a continuous conduit (Fig. 2; Shreve, 1972, 1985a; Anderson and Anderson, 2010). Such systematic variations in ridge CS dimensions and crest morphology have been observed in an assemblage of potential eskers in Argyre Planitia, Mars (Banks et al., 2009; Bernhardt et al., 2013).

3. Methods

3.1 Datasets and mapping

All Mars data were projected in ESRI ArcMap using a south polar stereographic projection. The latitude of zero distortion (standard parallel) was set to -74.5°S, approximating the centre of the Dorsa Argentea ridge distribution, reducing the estimated mean linear distortion error to ±0.6498 % over the study area (see S1 for error derivation). We created an image mosaic providing complete coverage (Fig. 3) of the Dorsa Argentea using ~6 m/pixel images in the 500 to 800 nm waveband from the Mars Reconnaissance Orbiter Context Camera (CTX) (Malin et al., 2007), with ~11-20 m/pixel panchromatic images from the Mars Express (MEX) High Resolution Stereo Camera (HRSC) (Neukum et al., 2004; Jaumann et al., 2007) in CTX data gaps (Refer to Table S2 for list of image products). We used the ~230 m/pixel and ~115 m/pixel-resolution gridded polar MOLA digital elevation model (DEM) products (Zuber et al., 1992; Som, 2008) to complement the image data. The ~230 m/pixel DEM was only used to provide coverage of the ridges in the most northerly latitudes of their distribution (Fig. 3). MOLA shot data (Precision Experiment Data Record, MGS-M_MOLA_3_PEDR_L1a-V1.0) were downloaded from the PDS Geosciences Node in shapefile format and overlain on the interpolated DEM to identify interpolated pixels in the MOLA DEM. Integration of image and topographic datasets improved confidence in mapping where either the image quality was poor, or where the DEM had been interpolated due to a low density of raw altimetry points.
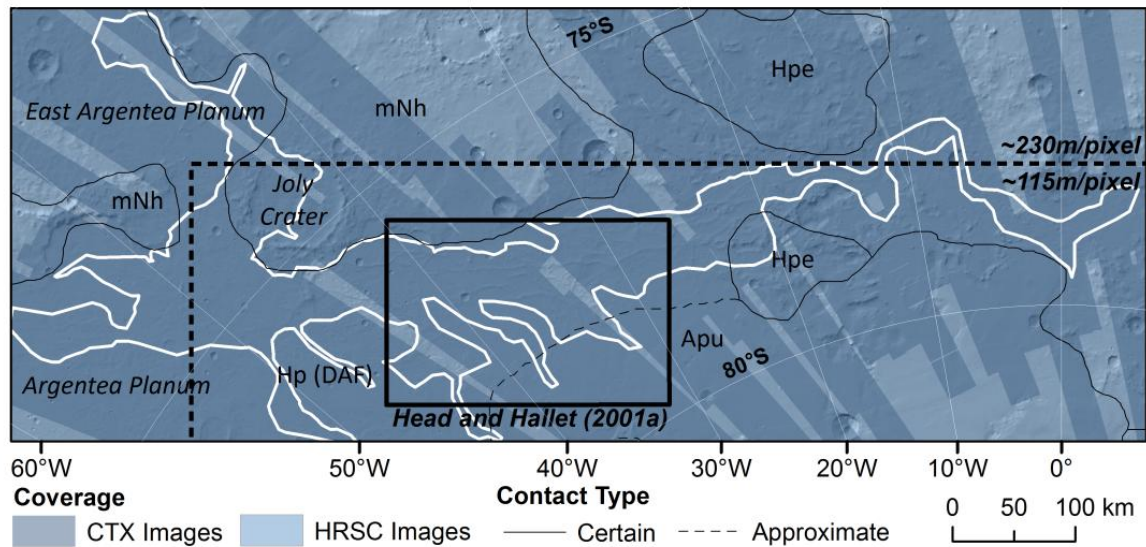
Figure *3: Data coverage map of the study region (extent displayed in Fig. 1) overlain on a hillshade map derived from the ~460 m/pixel MOLA DEM. The extent of the mapped ridges is outlined in white. The dashed line indicates the boundary between ~230m/pixel and ~115m/pixel MOLA DEMs. The solid box indicates the approximate study area of Head and Hallet (2001a). Projection is south polar stereographic. Surface units, labels and contacts are modified from Tanaka et al* (2014a).

Using this basemap, we digitised ridge *segments* in ArcMap with polylines following the ridge crest. Segments are defined as individual, unbroken ridges. We conservatively grouped ridge segments into longer ridge *systems,* defined as chains of ridge segments, separated by *gaps*, judged to be related on the basis of end-to-end proximity, orientation and visual similarity. Ridge *gaps* are defined as areas between ridge segments where elevations are similar to, or lower than the adjacent terrain. Segments that could not be related to systems >10 km in length (where distance is linearly interpolated across gaps) were excluded from the map as shorter features were not distinguishable from other 'hills', which can have similar aspect ratios. However, this conservative approach inevitably excluded some of the shortest ridges from the map. Mantled ridges extending northwards from the gradational contact with the Amazonian polar unit (Fig. 1) were only digitized if they formed clear continuation of an exposed ridge within the DAF.

13

Where segments branched or braided, we used visible continuation of ridge structure (e.g. layering in sloping sides) from up-ridge of a junction to classify ridge continuation. Where branches were similar, we classified the longest branch as the continuation of the primary ridge.

3.2 Planar ridge geometry

As illustrated in Fig. 4, we extracted the lengths of individual ridge segments (segment length, L_s), the total length of all segments in each ridge system (mapped length, L_m), and the total length of all segments plus the linearly interpolated distance across any gaps (system length, L_i) from the mapped polylines. Gradation of some ridge termini into the surrounding terrain introduced inaccuracies in their identification. The uncertainty arising from gradation of ridge termini into the surrounding terrain was approximated to be ±44 m, which is significantly smaller than the distortion error due to the projection (see S1).

Continuity (C) describes the degree of ridge fragmentation, defined as the ratio between L_m and L_i for each interpolated ridge.

Ridge segment sinuosity (S_s) is defined as the ratio between L_s and the shortest linear distance (path length, L_l) between the end points of a segment. We calculated sinuosity of interpolated ridges (S_i) in a similar manner, where L_l was calculated between the start and end points of each ridge system.
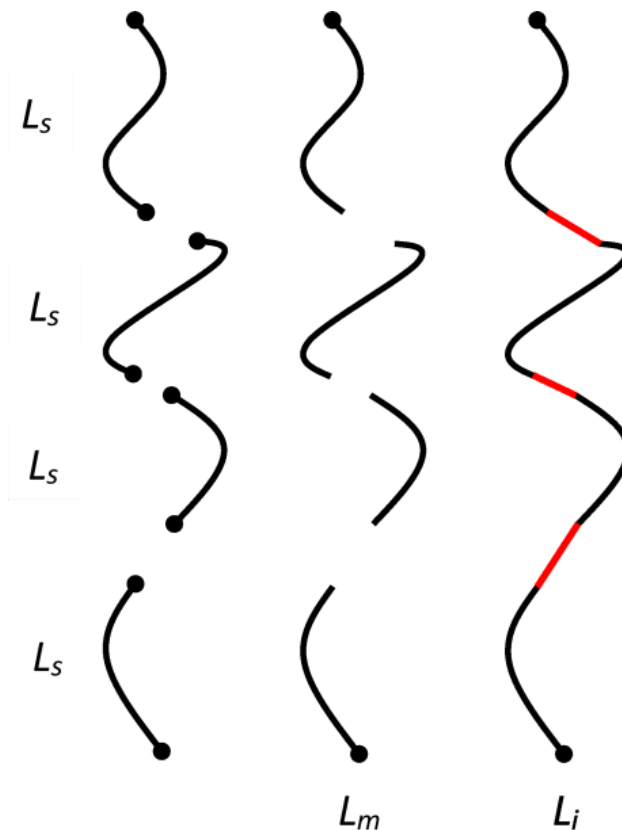
Figure 4: *Method for calculation of ridge segment length (Ls), mapped length (Lm) and system length (Li). Dots indicate the start and termination points of length calculations. Gaps in solid lines between points are not included in length calculations. Straight red lines indicate linear interpolation of length calculation across gaps.*

3.4 Definition of cross-sectional profiles

We sampled four major ridges, arbitrarily named A-D (Fig. 5), for analysis of the relationship of CS dimensions and crest morphology to topography. These ridges were sampled from the 50 longest interpolated ridge systems. Therefore, cross-sectional geometries reported in this study likely reflect the upper range for the Dorsa Argentea population. Sampling of longer ridges ensured sufficient data for statistically meaningful analyses of individual ridges. Furthermore, if the Dorsa Argentea are eskers, longer ridges are the most likely to have formed in stable R-channel networks in which conditions most closely approximate the assumptions upon which Shreve's (1972, 1985a, 1985b) theory is

based. Eskers formed in channels where the assumptions of Shreve's model are not met may not exhibit the topographic relationships which we sought to test in this study. The sampled ridges were spatially distributed throughout the DAF, and therefore adequately represented the whole Dorsa Argentea population.

The image mosaic was unsuitable for accurate identification of the ridge base due to the gradation of ridges into the surrounding terrain. Therefore, we obtained ~6 km-wide cross-sectional topographic ridge profiles with point spacing similar to the cell size of the ~115 m/pixel DEM at ~1 km spacing along mapped segments of the sampled ridges for measurement of CS dimensions, crest morphology and longitudinal bed slope. CS profiles were not taken within the lower resolution ~230 m/pixel DEM. CS profiles where MOLA shot point densities were low (fewer than 5 shots intersecting the ridge within 0.5km of the CS profile) were excluded to minimize the uncertainty from DEM interpolation. CS profiles superposed on ridge gaps, junctions, or impact craters were also excluded. Elevation values for points on the CS profiles (Z_{point}) were extracted from the MOLA DEM.

3.5 Cross-sectional dimensions and crest morphology

We calculated ridge height (H) and width (W) for each CS profile based on the geometry of ridge base (B_{left} and B_{right}) and crest points. Gentle gradation of side slopes and local topography introduced a degree of subjectivity to base point identification. To ensure consistency, the classification procedure was standardized as follows:
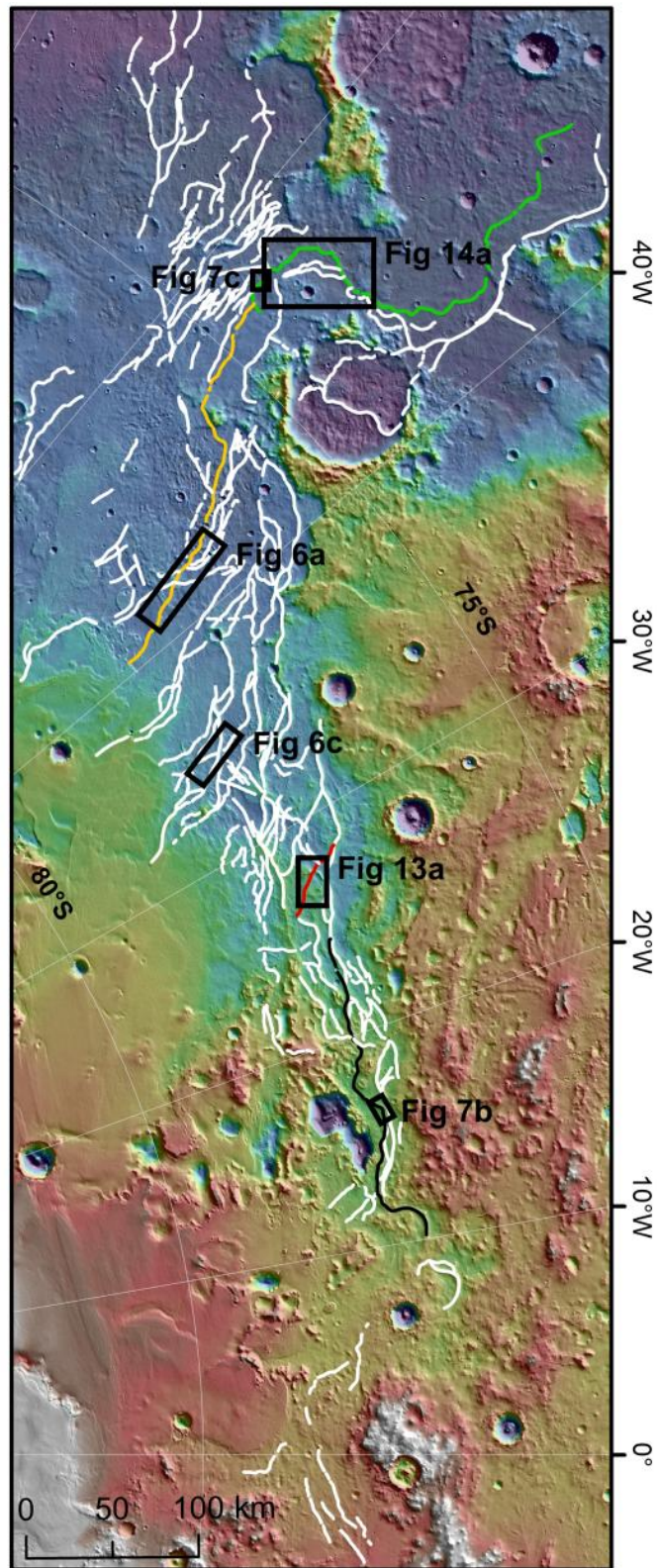
Ridges sampled for detailed analysis
— Ridge A   — Ridge C
— Ridge B   — Ridge D
MOLA Elevation (m)

2548 ▨ 23

Figure 5: Map of the Dorsa Argentea ridges showing the four ridges, A, B, C and D (highlighted) sampled for detailed analysis of cross-sectional dimensions, crest morphology and topographic relationships, overlain on a hillshade map derived from ~115 and ~230 m/pixel MOLA DEMs and colourised topography, also from these DEMs. Map extent is displayed in Fig. 1. Black boxes delineate the extents of subsequent figures. The reader is referred to the web-version of this article for interpretation of the colours in this figure.

1. CS profile points were overlain on the colourised MOLA DEM and candidate base points selected.

2. Points were then viewed in profile at fifty-times vertical exaggeration, and additional candidate base points selected based on breaks in slope.

3. Candidate points identified in (1) and (2) were then evaluated in plan-view on the integrated basemap, allowing contextualisation of topography and final classification of B_{left} and B_{right}.

We classified the crest as the highest point between B_{left} and B_{right}. Bed elevation (Z_{base}) was approximated as the mean elevation of B_{left} (Z_l) and B_{right} (Z_r). Ridge height (*H*) was calculated as the difference between the elevation of the crest point (Z_{crest}) and Z_{base}. Ridge width (*W*) was calculated as the distance between B_{right} and B_{left}.

The integrated basemap reveals emergence of Ridge C from a mantling deposit extending into the DAF from the Amazonian-aged polar unit in the south (Fig. 6a) up to 89 km along its length. Mann-Whitney U tests for difference in sample medians, the results of which are displayed in Table 1, indicate that mantled ridge sections typically have greater heights and widths than exposed sections. This indicates that CS dimensions and potentially crest morphology are modified significantly by the deposit, and justifies exclusion of mantled sections of Ridge C from analysis. Sections affected by remnant accumulations of the mantling deposit adjacent to Ridge C near to the contact with the mantle (Fig. 6b) were also excluded.

18

We classified CS profiles into the sharp, multiple and broad crest morphological types. These categories of crest morphology were identified by Shreve (1985a) for terrestrial eskers (see Section 2.2). CS profiles with multiple peaks were classified as multiple-crested.
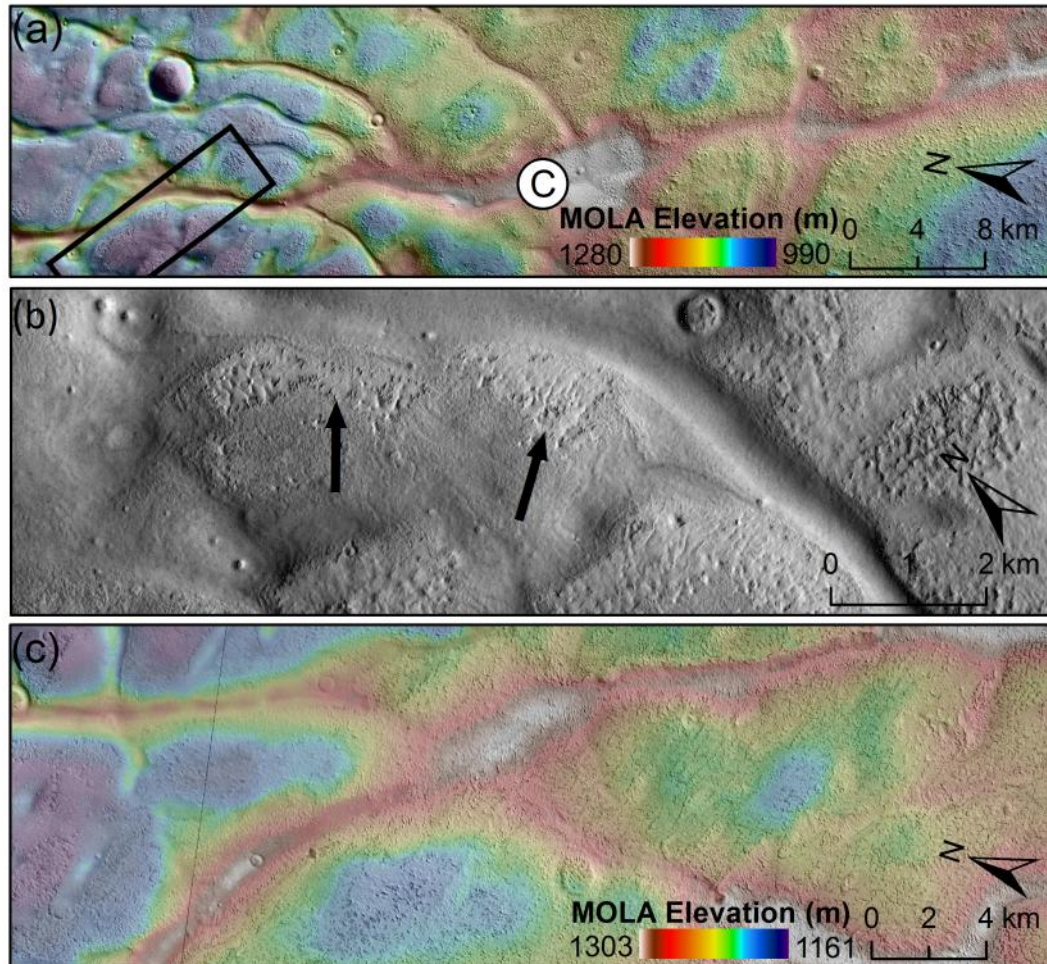
Figure 6: *Illustrations of the influence of the textured mantling deposit upon ridges within the study area. The reader is referred to the web-version of this article for interpretation of the colours in this figure. (a) CTX image P13_006282_1046_XN_75S043W overlain with colourised MOLA ~115m/pixel DEM showing emergence of Ridge C from textured mantling deposit in the South East. Black box shows location of (b). Extent shown in Fig. 5 (b) CTX image P13_006282_1046_XN_75S043W of a section of Ridge C close to the contact with the mantling deposit showing remnant accumulations (indicated by black arrows) of the textured deposit adjacent to Ridge C; (c) CTX image P12_005807_1024_XI_77S035W overlain with colourised MOLA ~115 m/pixel DEM showing mantling by the textured deposit*

19

of ridge intersection A referred to in Fig.5 of Head and Hallet (2001a). Extent shown in Fig. 5. CTX image credit: NASA/JPL-Caltech/MSSS.

Sharp and broad crests were distinguished using the criteria of Bernhardt et al. (2013) for putative eskers in Argyre Planitia, Mars, based on the cross-sectional slope at the crest. Across-ridge CS slope (θ_X), in degrees (°), was calculated from the difference in distance between successive points along the profile (*dMx*) and the change in elevation between those points (dZ_{point}). As illustrated in Fig. 7, CS profiles were classified as broad-crested where θ_X was <1° for three or more consecutive points (>~345 m), including the crest point, accounting for >10% of the average width of the sampled ridges. Single-crested profiles with crest slopes >1°, were classified as sharp-crested. Profiles of Z_{point} viewed alongside θ_X profiles (Fig. 7) confirmed effective distinction between visibly different crest morphological types under this classification scheme. It should be emphasised that these threshold criteria may not be directly applicable to terrestrial eskers, since differences in variables such as gravity between Earth and Mars are likely to result in variations in the vertical expression of the ridge crests, and by extension, the geometry that defines the threshold between 'sharp-crested' and 'broad-crested' esker sections. Given that classification of crest morphology in the present study is not undertaken for the purpose of comparing the raw geometries of sharp-crested and broad-crested sections to those on Earth, but instead for testing for esker-like differences in bed slopes occupied by sharp-crested and broad-crested sections of the Dorsa Argentea, we consider this to be an appropriate approach.

	Height, *H*		Width, *W*	
	Mantled	**Exposed**	**Mantled**	**Exposed**
n	58	63	58	63
Median (m)	47	36	3667	2669
KS-test value	0.097	0.155	0.072	0.112
KS-test p-value	>0.150	<0.010	>0.150	0.049
Mann-Whitney U Wilcoxon value (One-tailed, H_1 Mantled > Exposed)	4107		4613	
Mann-Whitney U p-value	0.0016		0.0000	

Table 1: Results of preliminary analysis of the effect of the textured mantling deposit upon cross-sectional dimensions of Ridge C using a Mann-Whitney U test for difference between sample medians. KS-test is Kolmogorov Smirnov test for normality.
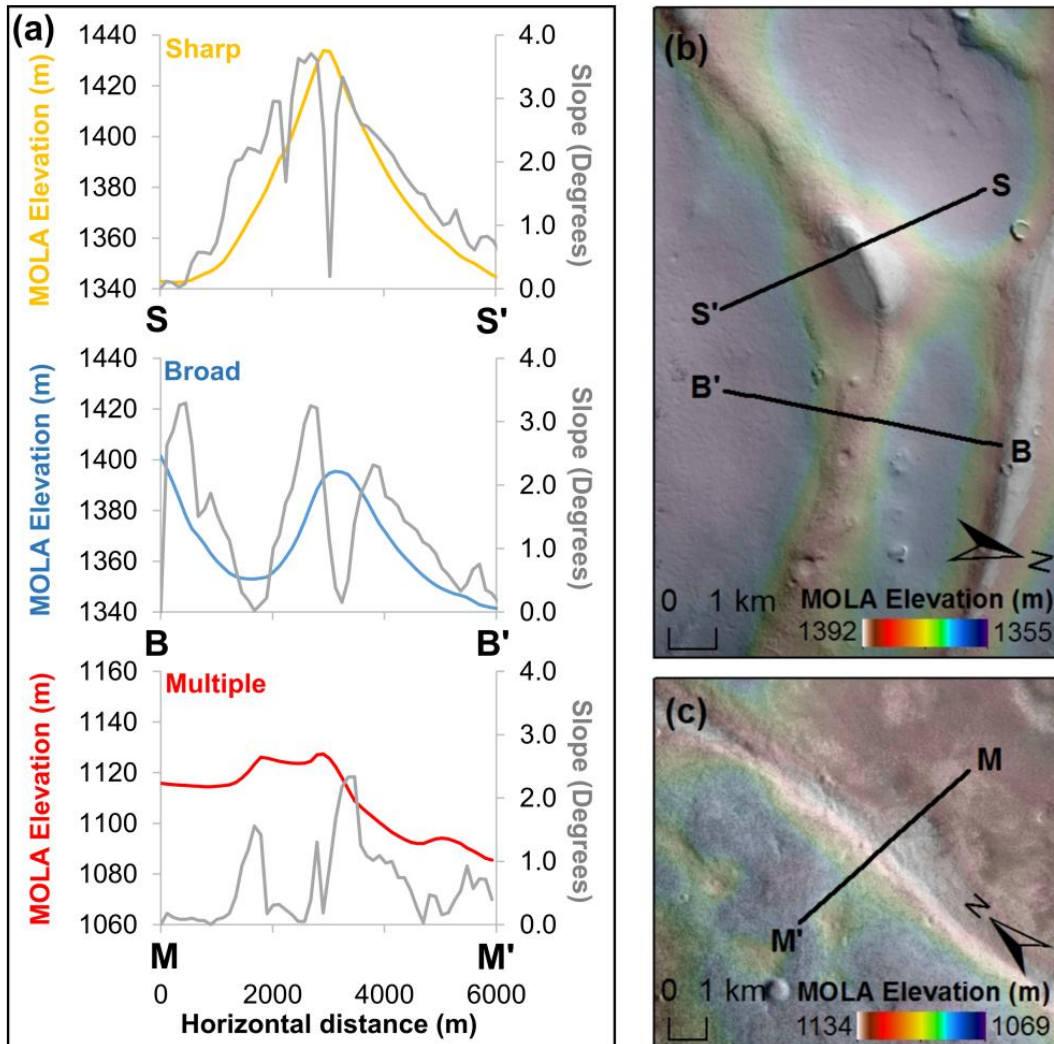
Figure 7: *Examples of classification of ridge crest morphological types. **(a)** Elevation (coloured lines) and slope (grey lines) profiles are displayed for sharp, broad, and multiple-crested crest morphologies. Letters refer to the start and end points of the profiles displayed in (b) and (c). Scales are equivalent on all three plots and have vertical exaggeration of ~46. Point spacing along profiles is ~115 m. **(b)** A section of Ridge D showing the locations of the sharp-crested and broad-crested cross-sectional profiles in (a). MOLA ~115m/pixel DEM overlain on CTX image B08_012610_1036_XN_76S018W, image credit: NASA/JPL-Caltech/MSSS. Extent displayed in Fig. 5. **(c)** A section of Ridge B showing the location of the multiple-crested cross-sectional profile in (a). MOLA ~115m/pixel DEM overlain on CTX*

image G13_023371_1065_XN_73S048W, image credit: NASA/JPL-Caltech/MSSS. Extent displayed in Fig. 5. The reader is referred to the web-version of this article for interpretation of the colours in this figure.

3.6 Longitudinal change in ridge height and bed slope

In order to test the relationship between the change in ridge height and longitudinal bed slope observed by Shreve (1985a) for terrestrial eskers, we calculated the difference between the height of each CS profile *(H_1)* and the height of the neighbouring up-ridge CS profile (*H_0)*, *dH*. We did not perform calculations of *dH* across ridge intersections as changes in ridge dimensions across esker junctions may be influenced by externally-driven changes in meltwater discharge at a conduit confluence, potentially reducing the clarity of any internally-controlled relationship that may exist if the Dorsa Argentea are eskers. We applied the same exclusion for analysis of relationships of crest morphology to topography.

We calculated longitudinal bed slope (θ_L), in degrees, between each CS profile and the preceding (up-ridge) CS profile based on the down-ridge change in Z_{base} (dZ_{base}) and the longitudinal distance (dM_L) between them. Ascending slopes are indicated by positive θ_L values and descending slopes by negative values.

The assumption of a consistent bed slope between sampled CS profiles may have overlooked sub-kilometre-scale variations in bed slope. However, the ~1 km spacing between profiles, which is small relative to the typical widths of the sampled ridges, is likely to have captured the basic characteristics of the surrounding topography, which has low levels of relief.

3.7 Uncertainties

Uncertainties in measured variables arising from known instrument inaccuracies, experimentally estimated distortion due to the projection, and methodological uncertainties were calculated based on propagation of errors for the most extreme values in the dataset and are displayed in Table 2. See Supplementary Material 1 for their derivation.

23

Quantity	Error
Segment length, L_s	± 973 m
Mapped length, L_m	± 5149 m
System length, L_i	± 5168 m
Continuity, C	± 0.02
Segment sinuosity, S_s	± 0.01
System sinuosity, S_i	± 0.03
Ridge base elevation, Z_{base}	± 0.707 m
Height, H	± 1.23 m
Width, W	± 141 m
Longitudinal change in ridge height, dH	± 1.74 m
Longitudinal bed slope, θ_L	± 0.1°

Table 2: *Estimations of uncertainties for calculated quantities based on propagation of errors for the most extreme values in the dataset (see S1 for derivation).*

4. Results

4.1 Planar ridge geometry

In total, we mapped ~6772 km of ridge segments (*n* = 720). Descriptive statistics for segment length (L_s), mapped length (L_m) and system length (L_i) are displayed in Table 3.

The distribution of L_s (Fig. 8a) is positively skewed, varying by three orders of magnitude from ~0.2 km, up to a maximum of ~150 km, with median ~4.8 km and mean ~9.4 km (Standard Error, S.E. = 495 m). Log-transformed L_s values ($log_{10}L_s$) have a normal distribution (Kolmogorov-Smirnov, KS-value = 0.03; p-value = 0.05) (Table 3). Segments less than 10 km in length account for ~27 % of total L_m, whilst those exceeding 50 km in length account for ~17 %. One mapped segment exceeds 100 km in length (~150 km), accounting for ~2 % of total L_m.

When considered as fragments of longer ridge systems (*n* = 206), the mapped ridges form a total L_i of ~7514 km (Table 3). Ridge systems extend up to ~314 km in length. The minimum recorded length of 10 km is likely an artefact of the 10 km L_i threshold for mapping, although there is little visual evidence for the existence of significantly shorter ridge forms. L_i is strongly positively skewed with median ~22 km and mean ~36 km with S.E. 2764 m.

	Segment Length, L_s	Mapped Length, L_m	System Length, L_i	Continuity, C	Segment Sinuosity, S_s	System Sinuosity, S_i
n	720	206	206	206	720	206
Total	6772 km	6772 km	7514 km	NA	NA	NA
Minimum	0.18 km	8 km	10 km	0.59	1.00	1.01
Maximum	150 km	260 km	314 km	1.00	1.75	1.91
Median	4.81 km	20 km	22 km	0.94	1.02	1.07
Mean	9.41 km	33 km	36 km	0.91	1.04	1.10
Standard Error	0.495 km	2.483 km	2.764 km	0.01	0.00	0.01
Standard Deviation	13.28 km	35.63 km	40 km	0.10	0.06	0.12
Skewness	4.10	3.30	3.37	-1.06	4.98	3.34
Kurtosis	29.29	16.57	18.92	3.51	36.80	14.25
KS-test value	0.24	0.246	0.253	0.171	0.284	0.216
KS-test p-value	<0.010	<0.010	<0.010	<0.010	<0.010	<0.010
Log_{10} KS-test value	0.03	0.093	0.096	0.185	0.266	0.186
Log_{10} KS-test p-value	0.05	<0.010	<0.010	<0.010	<0.010	<0.010

Table 3: *Descriptive statistics of planar geometry of mapped ridges*

A ratio of 0.91 between total L_m and total L_i indicates that the Dorsa Argentea have low degrees of fragmentation, with gaps accounting for ~10 % of L_i. On average, each ridge system is formed of 3.5 (standard deviation, S.D. = 3.2) segments. The distribution of continuity (C) values for ridge systems (Fig. 8b) is strongly negatively skewed with a median of 0.94 (Table 3). Ridge systems formed of a single segment ($C = 1$) account for ~30 % of mapped ridges. However, some ridge systems have higher degrees of fragmentation, with a minimum continuity of 0.59.
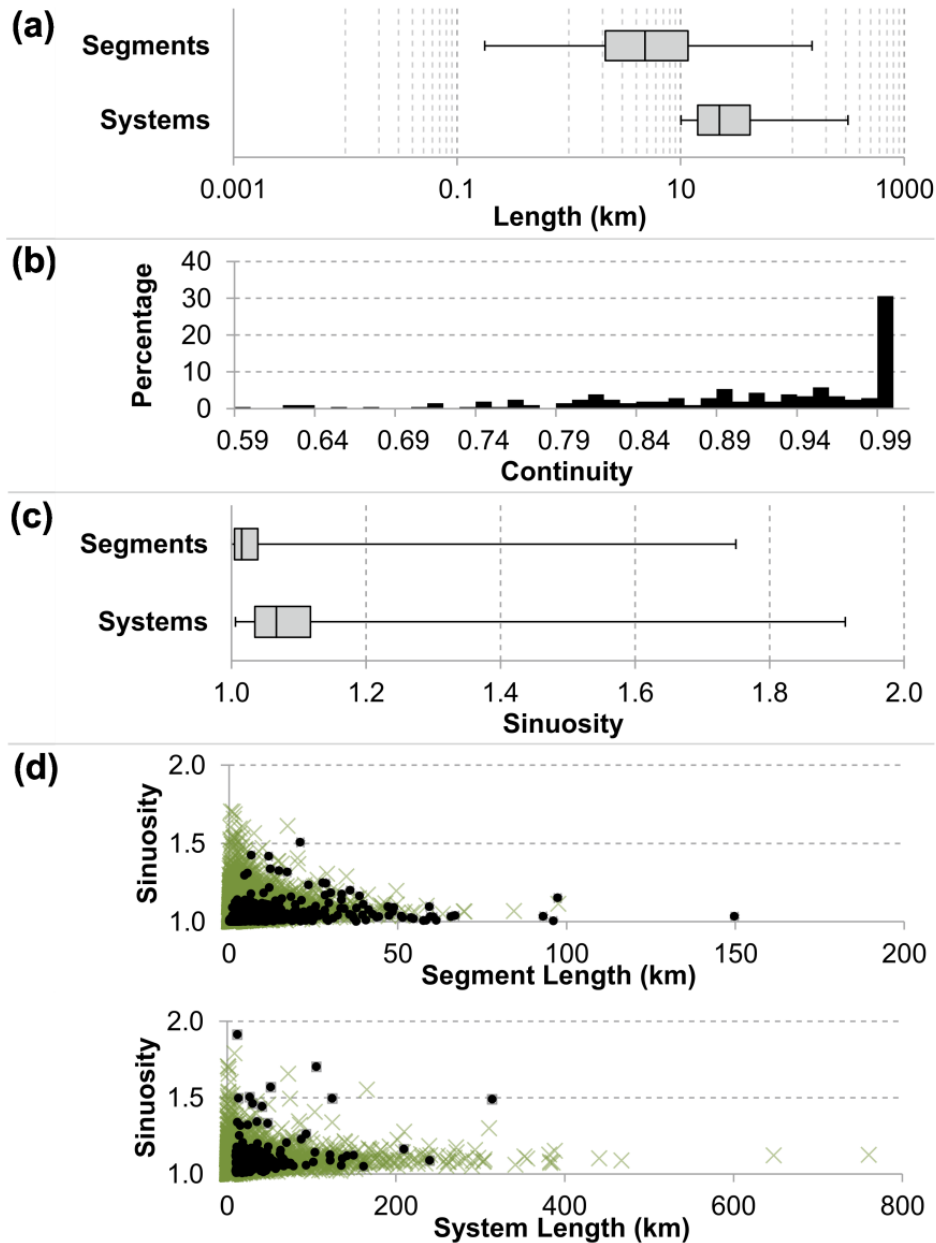
Figure 8: *Distributions of planar geometries of the Dorsa Argentea: **(a)** boxplots of segment length, L_s, and system length, L_i, on a log_{10} x-axis. Boxes indicate the upper and lower quartiles and vertical lines within boxes are median values; **(b)** histogram of continuity, C (bin width is 0.1) for ridge systems (n = 206); **(c)** boxplots of segment sinuosity, S_s and system sinuosity, S_i, on a linear x-axis. Boxes indicate the upper and lower quartiles and vertical lines within boxes are median values; **(d)** scatterplots of segment sinuosity, S_s versus segment length, L_s and system sinuosity, S_i versus system length, L_i, (points) overlain on values for the Canadian eskers (crosses) from (Storrar et al., 2014a).*

In the following description, system sinuosity (S_i) is reported with segment sinuosity (S_s) in brackets. As is summarised in Table 3 and shown in Fig. 8c, the Dorsa Argentea typically have low sinuosities ranging from near-linear with sinuosity 1.01 (1.00), to paths with sinuosity up to 1.91 (1.75). With a median of 1.02 and mean 1.04 (S.E. = 0.00), S_s is more strongly positively skewed (skewness = 4.98; kurtosis = 36.80) than S_i (skewness = 3.34; kurtosis = 14.25), with a median of 1.07 and mean 1.10 (S.E. = 0.01). Scatterplots of sinuosities against ridge segment and system lengths in Fig. 8d illustrate that long ridges are typically straighter than shorter ridges. A map of S_i, displayed in Fig. 9a illustrates that ridge systems at the entry to East Argentea Planum have higher S_i values (~1.48 to ~1.7) than those within the main valley (~1 to ~1.3). This contrast can be seen in Fig. 9b.

4.2 Cross-sectional dimensions and crest morphology

As summarized in Table 4, the four major ridge systems sampled from the Dorsa Argentea (Fig. 5) range between 1 and 107 m in height, with equivalent mean and median heights of 42 m (S.E = 1 m). The heights of the ridges have a range, on average, of 73 m (S.E. = 9 m) along their lengths.

Ridge width ranges between ~700 m and ~6000 m, with a mean width range of ~4400 m (S.E. = 180 m) along individual ridges, and mean and median widths of ~3000 m (S.E. = 83 m) and ~3100 m, respectively. Longitudinal variations in ridge widths are gradual. A scatterplot of ridge height and width displayed in Fig. 10 shows that there is a significant positive linear correlation between height and width with a Pearson's correlation coefficient of 0.76 (p-value = 0.00).

The CS profiles sampled from Ridges A, B, C and D (n = 211) are dominated by sharp crest morphologies (75 %), with broad crest morphologies accounting for 24 %. Multiple-crested morphologies account for <1 % (n = 2) of CS profiles and are excluded from further analysis. Owing to the small number of CS profiles with broad crest morphologies identified on individual ridges (three with n<15), we completed statistical tests for difference in CS

27

dimensions between sharp- and broad-crested CS profiles for the entire sample, rather than for individual ridges.

	Ridge A	Ridge B	Ridge C	Ridge D	All CSPs
n	29	29	63	90	211
Height, H					
Minimum (m)	21	7	1	8	1
Maximum (m)	77	71	75	107	107
Median (m)	50	28	36	47	42
Mean (m)	48	32	37	48	42
Standard Deviation (m)	17	13	23	20	21
Standard Error (m)	3	2	3	2	1
Skewness	-0.68	0.98	0.98	0.65	0.31
Kurtosis	-1.44	2.02	2.020	0.58	-0.18
KS-test value	0.190	0.143	0.155	0.155	0.051
KS-test p-value	<0.010	0.132	<0.010	<0.010	>0.150
KS-test interpretation	Not Normal	Normal	Not Normal	Not Normal	Normal
Histogram distribution	Bimodal	Normal	Bimodal	Bimodal	Bimodal
Width, W					
Minimum (m)	1124	1446	669	1114	669
Maximum (m)	5132	5812	5143	5999	5999
Median (m)	3552	2917	2669	3453	3143
Mean (m)	3425	3410	2516	2957	3083
Standard Deviation (m)	1115	1272	1048	906	1203
Standard Error (m)	207	236	132	96	83
Skewness	-0.68	1.11	0.08	0.02	0.14
Kurtosis	-0.39	0.98	-0.82	-0.90	-0.61
KS-test Value	0.115	0.147	0.112	0.098	0.063
KS-test p-value	>0.150	0.106	0.049	0.040	0.045
KS-test interpretation	Normal	Normal	Not Normal	Not Normal	Not Normal
Histogram distribution	Normal	Normal	Bimodal	Bimodal	Bimodal

Table 4: *Descriptive statistics of cross-sectional dimensions of cross sectional profiles on Ridges A, B, C and D.*
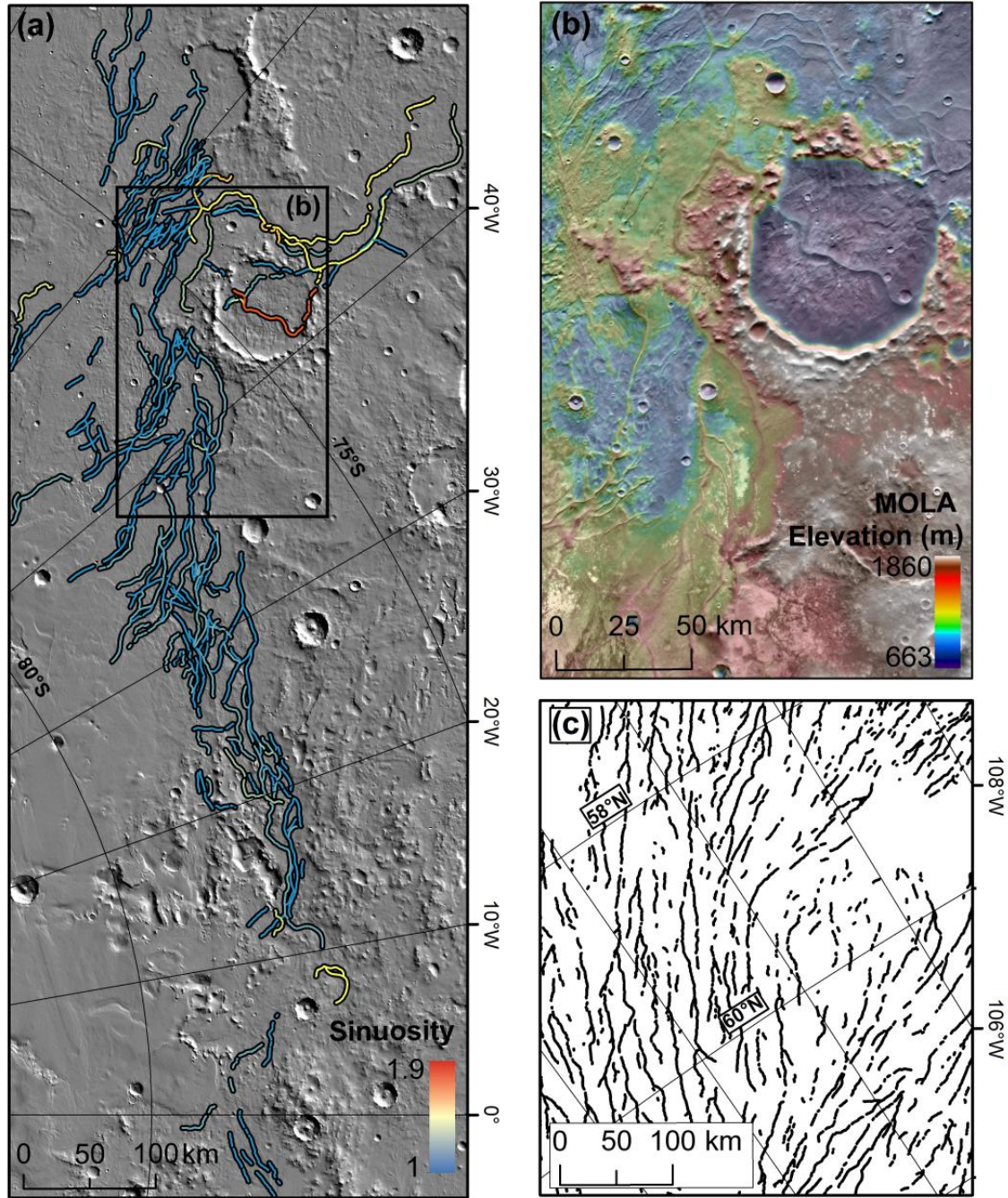
Figure 9: (a) Map of the Dorsa Argentea classified by system sinuosity, S_i overlain on a hillshade map derived from ~115 and ~230 m/pixel MOLA DEMs. Map extent is displayed in Fig. 1. (b) ~115 and 230 m/pixel MOLA DEM overlain on image from the ~100 m/pixel THEMIS Day IR v11 512ppd global mosaic from USGS (image credit: NASA/JPL-Caltech/Arizona State University) showing a region of the Dorsa Argentea. Extent displayed in (a). (c) Map of a region of the terrestrial eskers in Canada mapped by Storrar et al. (2013),

29

to which the Dorsa Argentea are compared in this study. The scale is similar to that in (a).

The reader is referred to the web-version of this article for interpretation of the colours in this

figure.

A one-tailed Mann-Whitney U test for difference in median heights (48 m and 30 m for sharp and broad crest morphologies, respectively) (Table 5) indicates that sharp crest morphologies typically have greater heights than broad crest morphologies, returning a Wilcoxon value of 18552 (p-value = 0.00).

In contrast, a two-tailed t-test (unequal variances) for normally-distributed widths indicates no significant difference in width between sharp (mean = ~3200 m; S.E. = 93 m) and broad (mean = ~2800 m; S.E. = 183 m) crest morphologies, returning a t-value of 1.51 which is insignificant at the 95 % level (p-value = 0.134) (Table 5).

These differences in dimensions are illustrated in Fig. 10 which indicates that sharp-crested ridge sections are generally taller relative to their widths than broad-crested sections, with differences in width-height ratios (Table 5) primarily arising from differences in height between crest morphological types. Significant difference in dimensions between sharp and broad crest morphologies, illustrated in Fig. 10, confirms the classification criteria made a meaningful distinction between crest morphological types.
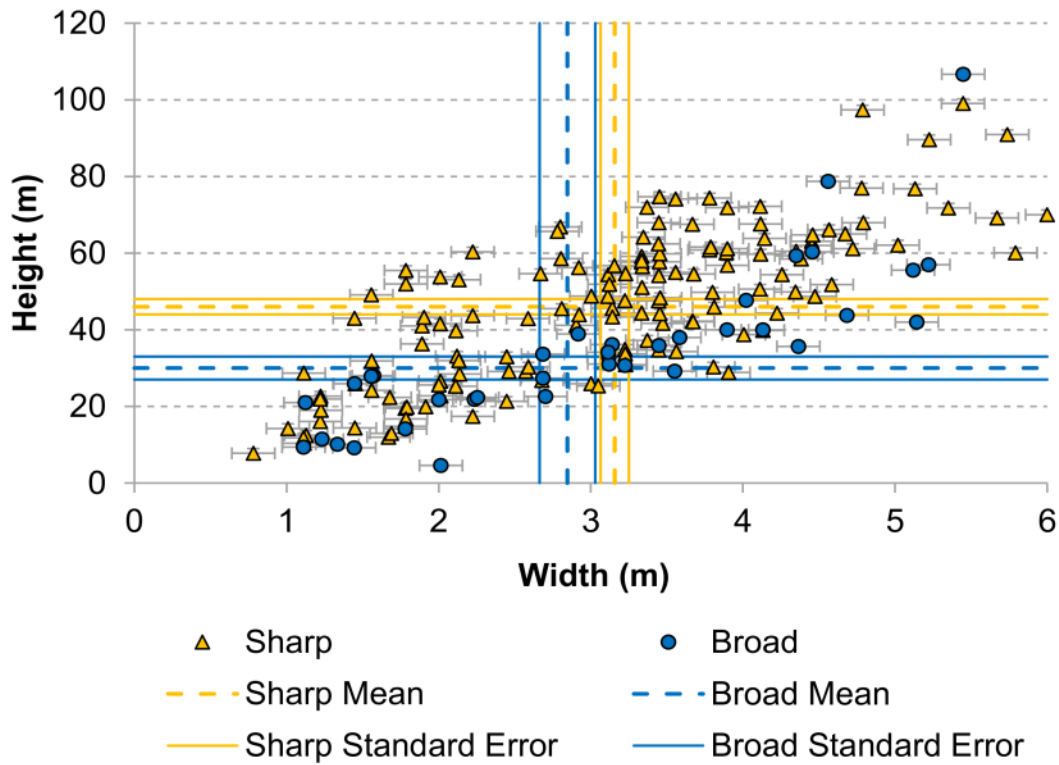
Figure 10: *Scatterplot of height, H against width, W, for ridge cross-sectional profiles, classified by crest morphological type. Error bars display uncertainties from Table 2.*

|	Height		Width		Width:Height	
	Sharp	**Broad**	**Sharp**	**Broad**	**Sharp**	**Broad**
n	159	50	159	50	159	50
Minimum (m)	8	1	781	669	32	51
Maximum (m)	99	107	5999	5448	176	721
Median (m)	48	30	3229	2904	69	101
Mean (m)	46	30	3157	2846	74	136
Standard Deviation (m)	20	20	1174	1295	24	124
Standard Error (m)	2	3	93	183	2	18
Skewness	0.13	1.31	0.15	0.23	1.02	3.29
Kurtosis	-0.39	3.44	-0.51	-0.92	1.55	11.35
KS-test value	0.059	0.132	0.066	0.098	0.101	0.351
KS-test p-value	>0.150	0.036	0.088	>0.150	<0.010	<0.010
KS-test interpretation	Normal	Not Normal	Normal	Normal	Not Normal	Not Normal
Mann-Whitney U Wilcoxon Value (One-tailed, H_1 Sharp > Broad)	18552		NA		NA	
Mann-Whitney U Wilcoxon Value (One-tailed, H_1 Sharp < Broad)	NA		NA		14399	
Two-tailed t-test t-value (Assuming unequal variances)	NA		1.51		NA	
Mann-Whitney U p-value	0.000				0.000	
Two-tailed t-test p-value			0.134			

Table 5: Descriptive statistics, and Mann-Whitney U tests for difference between sample medians, in ridge Height, H, Width, W and Width-Height Ratio between sharp and broad crest morphological types on Ridges A, B, C and D.

4.3 Topographic relationships

The ridges commonly ascend topographic undulations up to ~100 m high (e.g. Ridge D, Fig. 11). Fig. 11 shows that increases in bed elevation along the ridge profile are generally associated with decreases in ridge height and vice versa, as noted by Head and Hallet (2001a).

Simple bivariate plots of *dH* and θ_L are displayed in Fig. 12 and Pearson's correlation coefficients of -0.691 (p-value = 0.000) and -0.770 (p-value = 0.000) for Ridges A and B, respectively, indicate that these ridges strongly adhere to the negative correlation predicted by Shreve (1972, 1985a) for terrestrial eskers, with increases in ridge height on downhill slopes and decreases on uphill slopes. Ridges C and D exhibit weaker negative correlations with Pearson's correlation coefficients of -0.427 (p-value = 0.001) and -0.324 (p-value = 0.003) respectively.

We completed univariate ordinary least squares (OLS) regression analyses of θ_L (independent variable) and *dH* (dependent variable) for each of the ridges; the results are displayed in Table 6. θ_L explains 47.81 % (p-value-value = 0.000) and 59.26 % (p-value-value = 0.000) of the variance in *dH* along ridges A and B, respectively. θ_L is a relatively weak predictor of *dH* along ridges C and D, explaining 18.27 % (p-value = 0.001) and 10.47 % (p-value = 0.003) of its variance, respectively. Regression models were evaluated using the Moran's I statistical test for spatial autocorrelation, and a KS-test for normality, in regression residuals (Table 6). We computed spatial weights matrices for the Moran's I test on the basis of the euclidean distance to the centroids of the two nearest neighbouring CS profiles. Ridges A, B, C and D do not have statistically significant spatial autocorrelation and exhibit normality in their residuals, indicating robust model performance. Non-normality in

32
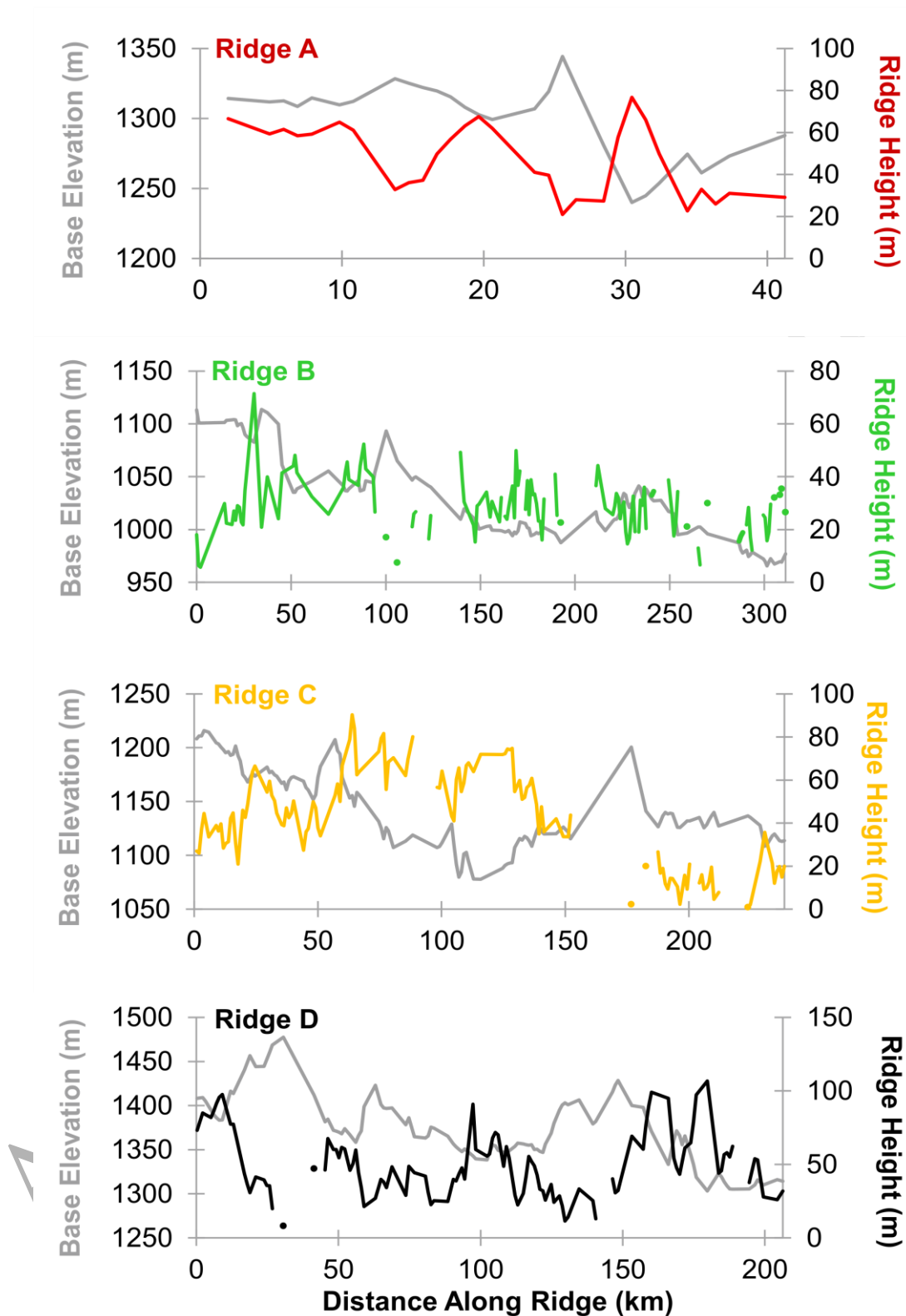
Figure 11: *Longitudinal plots of ridge height, H (coloured lines and points) and base elevation, Z_{base} (grey lines) derived from systematically sampled cross-sectional profiles on*

33

Ridges A, B, C and D. Gaps in ridge height profiles indicate gaps between ridge segments and points represent ridge segments along which a single cross-sectional profile was sampled. The profile for Ridge C includes the section mantled by the textured deposit (0-89 km) that is excluded from quantitative analysis. Note the different x- and y-axis scales.

	Ridge A (n = 28)		Ridge B (n = 20)		Ridge C (n = 55)		Ridge D (n = 80)	
Test of assumption of normality of dependent variable, dH. (P-value > 0.01 is normal)								
KS-test value	0.117		0.135		0.134		0.106	
P-value	>0.150		>0.150		0.021		0.034	
Assumption of normality	Valid		Valid		Valid		Valid	
Model								
R-squared	47.81%		59.26%		18.27%		10.47%	
F-Statistic	23.82		26.19		11.85		9.12	
P-value	0.000		0.000		0.001		0.003	
	Bed Slope	**Constant**	**Bed Slope**	**Constant**	**Bed Slope**	**Constant**	**Bed Slope**	**Constant**
Coefficient	-14.28	-2.47	-20.34	0.23	-9.29	-0.807	-14.60	-0.60
S.E. (Coefficient)	2.93	1.83	3.97	1.02	2.70	0.992	4.83	1.64
T-value	-4.88	-1.35	-5.12	0.22	-3.44	-0.81	-3.02	-0.36
P-value	0.000	0.189	0.000	0.826	0.001	0.420	0.003	0.716
Significantly different from zero?	Yes	No	Yes	No	Yes	No	Yes	No
Tests of model performance								
Moran's I test for spatial autocorrelation in OLS regression residuals (k-nearest neighbours, k=2)								
Moran's I statistic	-0.482		1.017		-1.895		-1.947	
P-value	0.630		0.309		0.058		0.052	
Spatial Autocorrelation?	No		No		No		No	
Test for normality of regression residuals (P-value > 0.01 is normal)								
KS-test value	0.167		0.154		0.075		0.125	
P-value	0.046		>0.150		>0.150		<0.010	
Normality of regression residuals?	Yes		Yes		Yes		No	

Table 6: *Ordinary least squares (OLS) regression analyses of longitudinal bed slope θ_L (independent variable) and longitudinal change in ridge height, dH (dependent variable) for Ridges A, B, C and D: tests of assumptions, results and tests of model performance.*
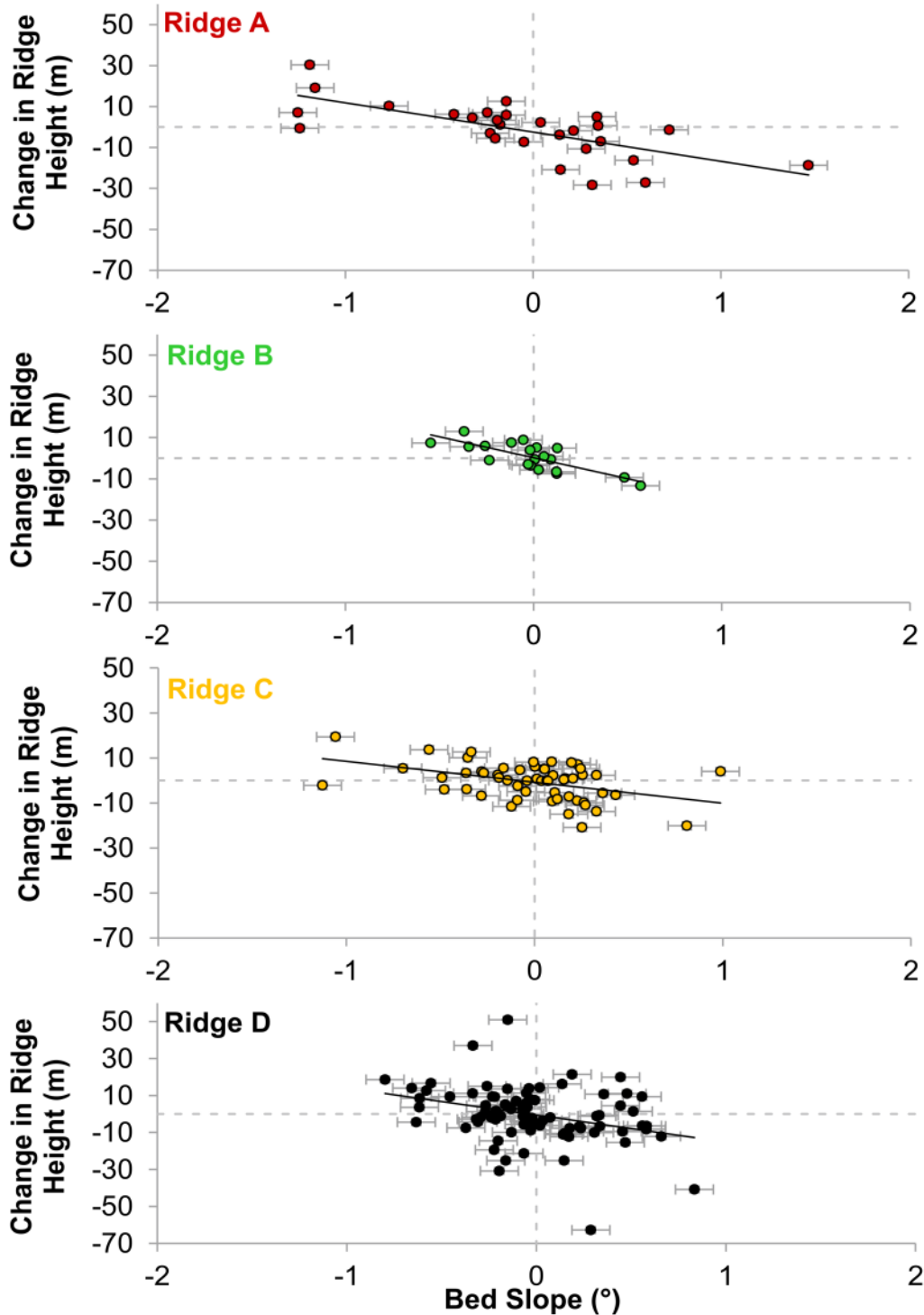
Figure 12: *Scatterplots of longitudinal change in ridge height (dH) against bed slope (θ_L) for cross-sectional profiles on Ridges A (n = 28), B (n = 20), C (n = 55) and D (n = 80), with linear trend lines. Upper left quadrants represent descending slopes and increasing ridge heights, and lower right quadrants represent ascending slopes and decreasing ridge height. Error bars display uncertainties from Table 2.*

regression residuals for Ridge D invalidates this model, indicating that other unidentified variables are required to explain variance in *dH* for this ridge. The relatively strong topographic relationships observed for Ridges A and B justify closer assessment of the character of these ridges.

Ridge A (L_i = ~47 km) passes northwest through an infilled (~10 km diameter) crater, traversing topographic lows in the degraded crater rim, as shown in Fig. 13a. The topographic profile of the crest of the crater rim in Fig. 13b intersects the ridge between sampled CS profiles at ~8 km, on the NW rim, and indicates that the ridge may have a gap that was undetected in the systematic CS profile sample, reducing to a negligible height as it passes over the crest. The ridge is well developed ($H ≈ 50$ m) over the more subdued topography of the SE rim (~22 km along profile). Infilling of small (sub-kilometre-scale) craters in CTX images indicate possible mantling of the ridge by a deposit (Fig. 13a) which may distort the true dimensions and topographic relationships of the underlying ridge. However, surface manifestation of the rims of small infilled craters indicates that this deposit is thinner than that mantling ridges in the south (Section 3.5, Fig 6) and may therefore have a more limited effect upon the dimensions of the underlying ridge.

Ridge B is the longest of the mapped ridge systems of the Dorsa Argentea (L_i = 314 km) and appears to be unaffected by the deposit that mantles Ridge A. It is the primary ridge passing into East Argentea Planum from the main valley, NW of Joly Crater, and has two major tributary ridge systems, forming a branching network (Fig. 14a). Close to the entry to East Argentea Planum, a pedestal feature, shown in Fig. 14a, extends laterally from an outer bend in the ridge. CTX images reveal layering in the sloping sides of some ridge sections (Fig. 14b), which may be continuous over distances of kilometres.

Equivalent medians of -0.03° in distributions of bed slopes occupied by sharp and broad crest morphologies indicate no discernible difference in bed slopes occupied by sharp

and broad crest morphological types. This is confirmed by a two-tailed Mann-Whitney U test,

(Table 7) which returns a statistically insignificant Wilcoxon value of 13254 (p-value = 0.964).
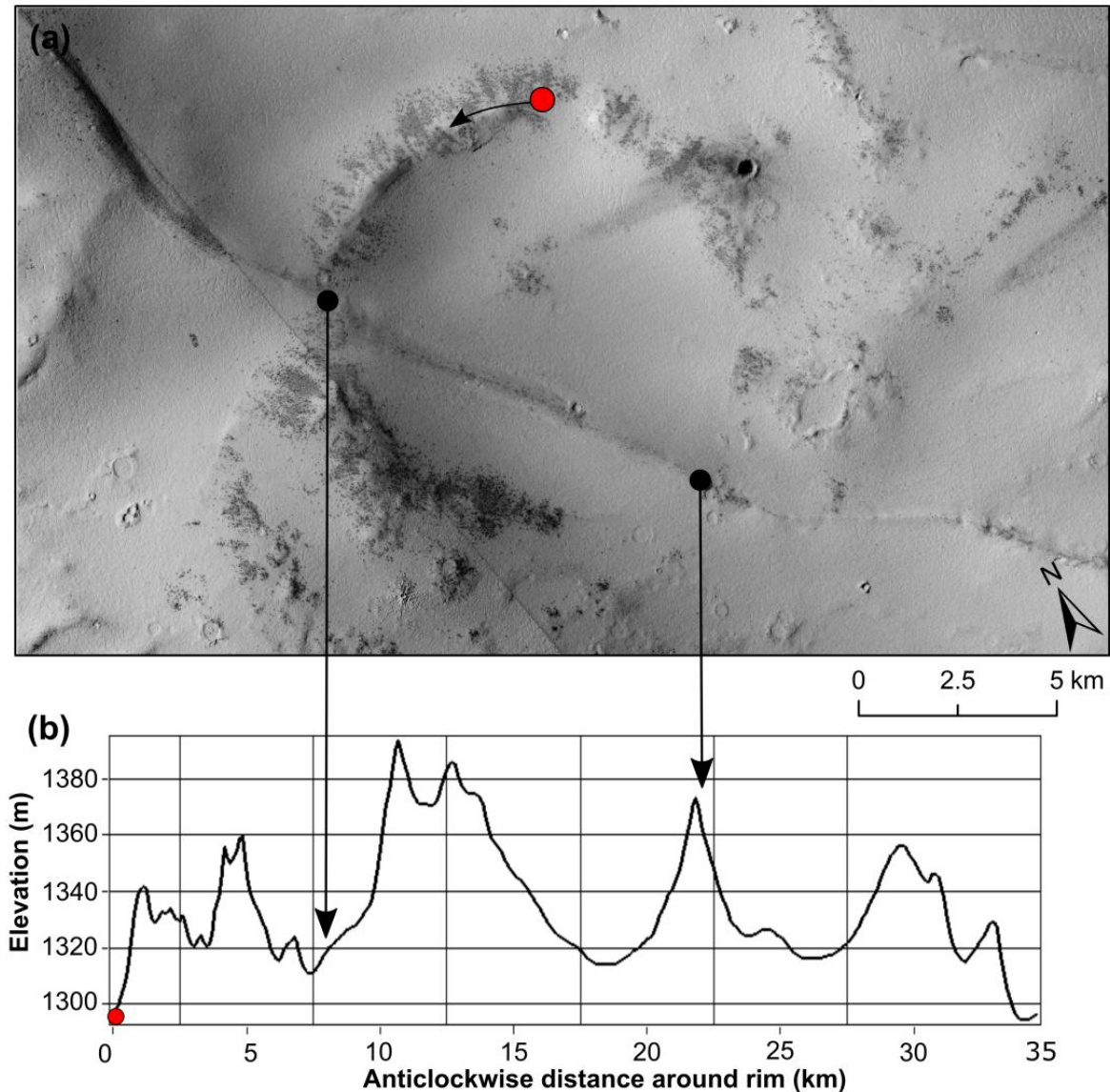
Figure 13 (a) *Passage of Ridge A through an infilled crater (CTX images B12_014_285_1025_XN_77S026W and B12_014351_1024_XN_77S028W, image credit: NASA/JPL-Caltech/MSSS). Image extent is displayed in Fig. 5. **(b)** Topographic profile of the crater rim derived from the ~115m/pixel MOLA DEM, passing anticlockwise from the point marked in (a). Points on the profile that intersect Ridge A are indicated with vertical arrows.*
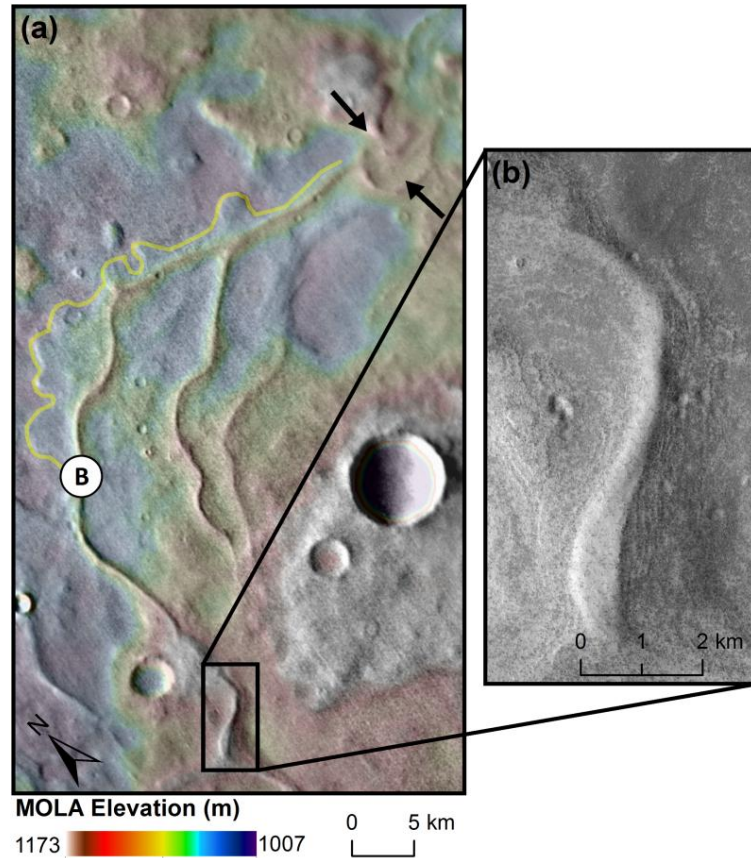
Figure 14: (a) *Image from ~100 m/pixel THEMIS Day IR v11 512ppd global mosaic from USGS (image credit: NASA/JPL-Caltech/Arizona State University) of a section of Ridge B (extent displayed in Fig. 5.) showing the lateral pedestal feature (outlined). Black arrows indicate entry of Ridge B into East Argentea Planum. The black box shows the extent of (b). The reader is referred to the web-version of this article for interpretation of the colours in this figure.* *(b)* *Evidence of layering structures in the side slopes of Ridge B (CTX image G13_023371_1065_XN_73S048W, image credit: NASA/JPL-Caltech/MSSS).*

	Sharp	Broad
n	145	37
Minimum (°)	-1.19	-1.25
Maximum (°)	0.9882	1.47
Median (°)	-0.03	-0.03
Skewness	-0.36	-0.03
Kurtosis	0.92	3.98
KS-test value	0.066	0.189
KS-test p-value	0.129	<0.010
KS-test interpretation	Normal	Not Normal
Mann-Whitney U Wilcoxon value (two-tailed)	13254	
Mann-Whitney U p-value	0.964	

Table 7: *Descriptive statistics for, and tests for difference between, longitudinal bed slopes occupied by sharp and broad crest morphologies.*

5. Analysis

5.1 Comparison to previous studies of the Dorsa Argentea

The lengths of the longest ridge systems mapped in the present study are consistent with the upper length range (hundreds of kilometres) identified for the Dorsa Argentea by previous workers (Howard, 1981; Metzger, 1992; Head and Pratt, 2001). Whereas previous assessments of planar geometries of the Dorsa Argentea have primarily been dependent upon low-resolution (~150-300 m/pixel) Viking Orbiter images, the inclusion of higher-resolution CTX images in the integrated basemap employed within the present study allows greater insight into the influence of shorter ridge systems upon the statistical distribution of ridge lengths. The mean interpolated length of ridge systems in the Dorsa Argentea from the present study (~37 km) is shorter than the lower-bounding length (~50 km) of the shortest ridges identified by Head and Pratt (2001) and significantly shorter than the mean length of 153 km stated by Metzger (1992) for the Dorsa Argentea and putative eskers in Argyre Planitia, combined.

The high continuity (mean = 0.91, S.E. = 0.01) of the ridge systems mapped in the present study is similar, though slightly lower, than the average continuity of 0.97 measured by Metzger (1992) using ~150 - 300 m/pixel Viking images. This may be attributed to the higher resolution of images employed in the present study, which allowed better identification of ridge gaps. Mean system sinuosity (1.10, S.E. = 0.01) is consistent with the value of 1.2 obtained by Metzger (1992). Although Kress and Head (2015) do not define whether their calculations of ridge sinuosity, which are based on higher-resolution data than those of Metzger (1992), are based on ridge segments or interpolated ridge systems, their value of mean sinuosity (~1.06) falls between those values (1.04 and 1.10, respectively) calculated in the present study, improving confidence in the results. However, whereas

Kress and Head (2015) assert that, on average, longer ridges in the Dorsa Argentea have higher sinuosity, plots of ridge segment sinuosity and ridge system sinuosity against ridge length in the present study (Fig. 8d) indicate that longer ridges generally have lower sinuosity than shorter ridges.

The ridges sampled in the present study have heights up to 107 m and widths up to ~6 km, towards the upper range of dimensions identified by previous workers (Head and Hallet, 2001b; Head and Pratt, 2001). Due to sampling of the longest ridges, CS dimensions presented here (Table 4) likely represent the upper range for the Dorsa Argentea population.

Previous work has shown that the Dorsa Argentea do not consistently follow the steepest topographic slope. Instead, they track along slopes and occasionally ascend topographic undulations (Howard, 1981; Head and Hallet, 2001a, 2001b). In a brief conference abstract that focussed on the relatively small region of the Dorsa Argentea demarcated in Fig 3, Head and Hallet (2001a) identified tendencies for increases in ridge height on descending slopes and decreases in ridge height on ascending slopes, consistent with formation in pressurised subglacial conduits (Shreve, 1985a; Head and Hallet, 2001b). OLS regression models of percentage longitudinal change in ridge height and bed slope for two of the sampled ridges (Table 6) provide quantitative statistical support for these observations. Sharp, multiple and broad crest morphological types identified within the present study are consistent with the type 1, 2 and 3 ridge morphological types identified by Head and Hallet (2001a) for the Dorsa Argentea. However, preferential occurrence of multiple and broad crest morphologies on ascending slopes, compared to sharp crest morphologies in regions of low regional slope, as identified by Head and Hallet (2001a), is not supported by the quantitative analysis presented here. No discernible difference is found between bed slopes occupied by ridge sections with sharp and broad crest morphologies. The difference between our findings, and those of Head and Hallet (2001a) may be caused by the threshold criteria selected in this study to distinguish between sharp and broad crest morphologies. It could also show that the relationship is weaker than that study suggests. CTX images reveal a textured deposit which extends from the gradational boundary of the

Amazonian polar undivided unit (Tanaka et al., 2014a) and mantles the specific ridge sections to which Head and Hallet (2001a) refer (Fig. 6c). This mantle significantly alters the dimensions of the ridges (Table 1) and may also affect their crest morphology. Draping of this mantle over underlying topography may broaden the surface expression of the underlying ridge as it passes over a topographic obstacle, particularly if that topographic obstacle is oriented perpendicular to the path of the ridge, as in the example used by Head and Hallet (2001a) (Fig. 6c). This suggests the relationship between ridge crest morphology and bed topography for the Dorsa Argentea may not be as strong as previously suggested.

5.2 Previous comparisons to terrestrial esker analogues

Comparisons of planar geometries of the Dorsa Argentea to terrestrial esker analogues have previously been limited by a paucity of quantitative data for a large (ice-sheet-scale) sample of terrestrial eskers. As a result, previous studies have been limited to comparison of geometries of the Dorsa Argentea to simple descriptions of planar geometries of relatively small esker assemblages such as an assemblage of 130 eskers in New York State, USA (Metzger, 1992, 1991; Kargel and Strom, 1992), and the Katahdin esker system in Maine, USA (Kargel and Strom, 1992; Head, 2000a; Head and Hallet, 2001a, 2001b; Head and Pratt, 2001; Kress and Head, 2015), which comprises one major esker with five tributaries (Shreve, 1985a).

Metzger (1991, 1992) identified similarities in sinuosity between terrestrial eskers in New York State, USA and the Dorsa Argentea. These similarities have more recently been corroborated by Kress and Head (2015). However, Metzger (1991, 1992) acknowledge that the lower average length (~8.2 km) and continuity (~64 %) of these terrestrial eskers, relative to the Dorsa Argentea, limits their applicability as analogues.

In a comparison to morphological descriptions by Brennand (2000) of eskers formed beneath the Laurentide Ice Sheet, Kress and Head (2015) support similarities in planform map patterns, dimensions and sinuosity between long, sinuous and continuous ridges of the

Dorsa Argentea and terrestrial eskers formed in efficient channelised subglacial drainage conduits (R-channels, see Section 2.1).

However, they also distinguish a second population of ridges in the Dorsa Argentea which are shorter (kilometres to tens of kilometres in length) and more polygonal in their configuration than the long, sinuous and continuous ridges, and occur in regions between them. They propose that these ridges were formed by deposition in less efficient, 'slow' drainage systems (Fountain and Walder, 1998) in inter-R-channel areas of the bed. In 'slow', or 'distributed' drainage networks, water flows along narrow orifices between linked basal cavities which form as a result of glacial flow over topographic irregularities in the bed (Kamb, 1987). Terrestrial analogues for eskers formed in distributed systems do not exist, since eskers, by definition, form in channelised drainage systems rather than distributed systems. The most similar terrestrial eskers to which Kress and Head (2015) refer are short and deranged type III eskers as classified by Brennand (2000). The drainage systems in which these eskers form are characterised by short R-channels draining into interior lakes or channels incised into the bed (Brennand, 2000), and are therefore different to the distributed networks in which Kress and Head (2015) propose the shorter, polygonal ridges of the Dorsa Argentea formed.

The recent survey by Storrar et al. (2014a) of >20 000 terrestrial eskers in Canada provides the most extensive and detailed quantitative characterisation of terrestrial eskers to date. This provides a new opportunity for more detailed quantitative comparison of planar geometries of the Dorsa Argentea to terrestrial esker analogues. Although it is possible that the ice-sheet scale survey presented by Storrar et al. (2014a) may comprise eskers formed in heterogeneous drainage configurations over the bed of the Laurentide Ice Sheet, no such distinctions were made. Therefore, in absence of a terrestrial analogue to eskers formed in distributed networks, the present study does not distinguish between the long, sinuous and continuous, and short polygonal ridge populations described by Kress and Head (2015). The 10 km threshold for mapping means that the sample of Dorsa Argentea ridges is likely to be dominated by the population of longer ridges. The Dorsa Argentea may represent a single

42

sector of a formerly more extensive south polar ice sheet on Mars beneath which several populations of putative eskers formed (Kress and Head, 2015), whereas the data for the Canadian eskers represents the population at the scale of an entire ice sheet. Therefore, if processes of formation of the Canadian eskers and the Dorsa Argentea are similar, the planar geometries of the Dorsa Argentea may be expected to fall within the range of geometries represented by the Canadian eskers.

No large-scale quantitative characterisation similar to that of Storrar et al. (2014a) has yet been completed for cross-sectional characteristics of a large sample of terrestrial eskers. Therefore, comparison of quantitative characterisations of CS dimensions and crest morphology of the Dorsa Argentea to terrestrial analogues remains limited to relatively simple descriptions provided in smaller-scale terrestrial studies such as that of Shreve, (1985a) for the Katahdin esker system in Maine. Whilst the heights of the Dorsa Argentea are of the order of those of the Katahdin esker system, the Dorsa Argentea typically have widths an order of magnitude greater (1000s metres) and therefore significantly lower CS slopes, limiting its applicability for direct comparison of ridge cross-sectional dimensions. However, given that Shreve (1985a) explains topographic relationships for esker CS dimensions and crest morphology of the Katahdin esker system in terms of glacier physics, the Katahdin esker system remains as a suitable analogue with which to compare tests of these relationships for the Dorsa Argentea, assuming that the physics of meltwater flow in glaciers can be translated to Mars. Therefore, while quantitative characterisations of CS dimensions and crest morphology may provide useful comparison to large-scale analyses of CS-dimensions and crest morphologies of terrestrial eskers in the future, their primary contribution to the present study is in tests for esker-like longitudinal changes in ridge CS dimensions and crest morphology with bed slope.

5.3 Comparison to terrestrial analogues

Planar geometry statistics for the Dorsa Argentea are compared with those of >20 000 terrestrial eskers in Canada (Table 8, Fig. 9c). Whilst segment lengths of Dorsa Argentea are typically two to three times those of the Canadian eskers, the interpolated length of the longest ridge system of the Dorsa Argentea (L_i~314 km) is less than half that of the longest Canadian esker system (760 km).

Lengths of individual ridge segments of the Dorsa Argentea have a similar log-normal distribution to that of Canadian esker segments, which Storrar et al. (2014a) attribute to fragmentation of esker systems into shorter segments. The weaker positive skew of the distribution of segment lengths for the Dorsa Argentea may result from the difference in continuity between the Dorsa Argentea (0.91) and the Canadian eskers (0.65). The similarities in statistical distributions of ridge length indicate that the ice-sheet scale data for the Canadian eskers can be appropriately compared to possible ice-sheet-sector scale data in tests of the esker hypothesis for the Dorsa Argentea.

Mean sinuosity of ridge segments in the Dorsa Argentea (1.04, S.E. = 0.00) is similar to that of Canadian eskers (1.06) (Storrar et al., 2014a). Interpolated ridges of the Dorsa Argentea also have similar mean sinuosity (1.10, S.E. = 0.01) to the Canadian eskers (1.08). The small difference between these values may reflect the lower proportion of the length of the Dorsa Argentea that is accounted for by linearly interpolated gaps, owing to their higher continuity. Lower sinuosity of ridge segments relative to interpolated ridges is an outcome of fragmentation of more sinuous ridges into shorter, straighter segments (Storrar et al., 2014a). The maximum sinuosity observed for the Dorsa Argentea (1.91) falls within the upper bound of sinuosity recorded for the Canadian eskers (2.45, Table 8).

	Canada	Dorsa Argentea
Continuity	0.65	0.91
Segments		
Sample size, *n*	20718	720
Mean length (km)	3.5	9.4
Median length (km)	2.1	4.8
Maximum length (km)	97.5	149.8
Skewness (length)	4.57	4.10
Mean sinuosity	1.06	1.04
Median sinuosity	1.04	1.02
Maximum sinuosity	2.21	1.75
Systems		
Sample size, *n*	5932	260
Mean length (km)	15.6	36.5
Median length (km)	4.1	22.2
Maximum length (km)	760	313.9
Mean sinuosity	1.08	1.10
Median sinuosity	1.06	1.07
Maximum sinuosity	2.45	1.91

Table 8 *Comparison of planar geometry statistics for the Dorsa Argentea with those published by Storrar et al. (2014a) for terrestrial eskers in Canada. Data in column 1 is from Storrar et al. (2014a).*

Plots of sinuosity and ridge length for the Dorsa Argentea are more consistent with those presented by Storrar et al. (2014a) for the Canadian eskers (Fig. 8d) than with the assertion of Kress and Head (2015) that longer (>50 km) ridges of the Dorsa Argentea are more sinuous than shorter ridges.

The mean height (42 m, S.E = 1 m) for the sampled ridges is similar to heights of the largest terrestrial eskers (Shreve, 1985a; Clark and Walder, 1994). The positive correlation between ridge height and ridge width (Fig. 10) is similar to that observed by Storrar et al. (2015) for eskers on the foreland of Breiðamerjökull in Iceland, although width-height ratios are greater for the Dorsa Argentea. Although their mean width (3083 m, S.E = 83 m) is an order of magnitude greater than widths of typical terrestrial eskers (Shreve, 1985a; Clark and Walder, 1994), kilometre-scale widths have been observed for some terrestrial eskers (Banerjee and McDonald, 1975). Paleo-eskers in Mauritania have widths up to 1.5 km and heights between 100 and 150 m (Mangold, 2000). Many terrestrial eskers have significantly lower width-height ratios and, by extension, steeper side slopes than those observed for the

Dorsa Argentea. For example, eskers with mean lengths of tens of metres on the foreland of Breiðamerjökull in Iceland typically have widths only five times greater than their heights, both of which are typically <10 m, yielding average side slopes of ~11° (Storrar et al., 2015). However, given that the maximum length of these eskers (684 m) is significantly shorter than the lengths and widths of the Dorsa Argentea ridges sampled in the present study, they may not serve as suitable analogues. Furthermore, some terrestrial eskers have side slopes of a similar magnitude (<4°) to those observed for the Dorsa Argentea (Fig. 7a). According to Shreve (1985a), broad-crested eskers in eastern Maine have typical widths of ~600 m and heights of ~10 m. This yields an average side slope of ~1.9° which is within the range of side slopes observed for the Dorsa Argentea (Fig. 7a). The Peterborough esker in Canada has a maximum width of 1 km and a maximum height of 20m (Banerjee and McDonald, 1975), yielding a maximum average side slope of 2.3° at the widest point. As highlighted by Shreve (1985a), such ridge sections may not be distinguishable on the ground from other positive-relief landforms with low slopes, such as fans and deltas.

Statistical tests indicate that three of four of the Dorsa Argentea ridges exhibit statistically significant decreases in ridge height on ascending bed slopes and increases in ridge height on descending bed slopes, akin to the relationship described by Shreve (1985a) for the Katahdin esker system. The observed reduction to near-negligible height of Ridge A as it traverses the crest of a degraded crater rim (Fig. 13b), is consistent with observations of the Katahdin esker system as it passes over topographic obstacles (Shreve, 1985a).

Similarly to the terrestrial Katahdin esker system (Shreve, 1985a), sharp crest morphologies dominate the ridge systems sampled from the Dorsa Argentea. Significant differences in height between ridge sections characterised by sharp and broad crest morphologies are similar to those observed for terrestrial eskers. However unlike in the Katahdin system, no significant difference is found in the present study between bed slopes occupied by sharp- and broad-crested sections of the Dorsa Argentea ridges.

6. Discussion

6.1 Planar ridge geometry

The considerably higher continuity of the Dorsa Argentea relative to the Canadian eskers has several possible explanations. The lower resolution of the ~15 to ~30 m Landsat 7 Enhanced Thematic Mapper + (ETM+) images used by Storrar et al. (2013) to map the Canadian eskers may have resulted in exclusion of small esker segments in ridge gaps, thereby resulting in lower continuity values. However, it is unlikely that this provides the primary explanation for the great difference in continuity between the two ridge populations. The very low erosion rates of 0.02-0.03 nanometres per year that have prevailed on Mars since the formation of the Dorsa Argentea are several orders of magnitude lower than terrestrial erosion rates (Carr and Head, 2010), thereby potentially limiting the degree of post-formation fragmentation that may have occurred relative to the more fragmented eskers in Canada. A third explanation may be differences in their mechanism of formation, as will now be discussed.

The spatio-temporal nature of esker formation is a topic of ongoing debate within the terrestrial literature (e.g., Banerjee and McDonald, 1975; Brennand, 1994; Brennand and Shaw, 1996; Punkari, 1997; Brennand, 2000; Mäkinen, 2003; Hooke and Fastook, 2007; Storrar et al., 2014a). Explaining the formation of terrestrial eskers by synchronous deposition in long, continuous R-channels is complicated by a tendency for instability of these conduits beneath thick ice towards the interior of a glacier or ice sheet, which may preclude long-term sediment accumulation (Röthlisberger, 1972; Hooke and Fastook, 2007). Reduced discharge through subglacial R-channels, for example due to winter cessation of meltwater production, may cause periodic shutdown of R-channels extending towards the ice interior as opposition to ice creep closure by conduit water pressure is weakened (Hubbard and Nienow, 1997; Benn and Evans, 2010). Furthermore, negative temperature gradients between pressurised and geothermally-heated ice at the bed, and the surface of non-temperate ice masses, are steepened by the vertical growth of meltwater conduits at the

bed. This may result in more rapid conduction of heat to the overlying ice from the roof of the conduit, which exists at the pressure-melting point, thereby damping roof melting. Unless a critical threshold of viscous heat production (which is proportional to discharge) is reached at the conduit roof, formation of R-channels beneath thick ice may be inhibited (Hooke and Fastook, 2007). However, as the overlying ice thins towards the terminus, the temperature gradient between the base of the ice and its surface approaches zero and the damping of conduit growth theorised by Hooke and Fastook (2007) reduces, allowing growth of R-channels and sedimentation to occur, forming eskers. Therefore, many authors (e.g., Banerjee and McDonald, 1975; Punkari, 1997; Mäkinen, 2003; Hooke and Fastook, 2007; Storrar et al., 2014a) argue that long eskers may form by a time-transgressive mechanism, whereby eskers progressively extend up glacier as the thin terminal zone of an ice sheet retreats across the landscape. Eskers are most likely to form during periods of relative stability in the position of the ice terminus. During periods of more rapid retreat, the time available for esker sedimentation at the margin is more limited, resulting in gaps between esker segments (Storrar et al., 2014a).

Storrar et al. (2014a) support time-transgressive formation in temporally and spatially stable conduits at the retreating ice margin of an active ice sheet as the most likely explanation for the great length (>100 km) of many Canadian eskers. They suggest that the relationship between ridge length and sinuosity observed for the Canadian eskers (Fig. 8d) provides support for this formation mechanism. They theorise that pressurised water in long conduits extending into the interior of an ice sheet tends to follow straighter paths than water closer to atmospheric pressure in shorter conduits at a receding ice margin, where ice is thinner and bed topography exerts a stronger control over water flow (Storrar et al. 2014a).

If this theorised relationship is correct, the similar relationship between sinuosity and ridge segment and system lengths observed for the Dorsa Argentea (Fig. 8d) may therefore support time-transgressive formation at a retreating ice margin (Storrar et al., 2014a). Hooke and Fastook (2007) presented a theoretical mechanism by which segments of eskers formed

48

during sequential stages of ice retreat may align and potentially form continuous unbroken ridges. However, the continuity of the Dorsa Argentea ridges is extremely high and may be inconsistent with formation at a mobile ice margin, the position of which may fluctuate and result in post-depositional fragmentation of esker sediments (Brennand, 2000; Storrar et al., 2014a). As is argued by Kress and Head (2015), the high continuity may be more consistent with type 1 terrestrial eskers described by Brennand (2000), formed synchronously in long, stable R-channels extending from the interior of a former, likely stagnant, ice sheet and terminating in a standing water body at its margin. Maintenance of high conduit water pressures through hydraulic damming from a proglacial water body, downstream blockage by localised sediment damming or channel shutdown, or maintenance of discharge exceeding the threshold for conduit collapse may provide mechanisms promoting long-term stability of long, esker-forming R-channels beneath thick ice. Ice surface slopes of ~0.06° reconstructed from the paths of the Dorsa Argentea by Scanlon and Head (2015), geomorphological evidence for a paleolake in Argentea Planum (Head and Pratt, 2001), and evidence for fan-forms at the termini of ridges entering this region (Scanlon and Head, 2015) are consistent with this mode of formation. Furthermore, no moraine-like ridges representing the locations of successive still-stands of the terminus of an ice sheet have been identified within the Dorsa Argentea, suggesting that ice may not have retreated across the region of the Dorsa Argentea while wet-based conditions existed that may have been capable of mobilising moraine-forming sediments. We observe consistently low sinuosity of both long and short ridges in the main basin (Fig. 9a), and higher sinuosity of the northernmost ridges (including Ridge B) at the entry to East Argentea Planum (Fig. 9a, Fig. 9b). We suggest that this may indicate that ridges in the main basin formed beneath thick ice towards the interior of a former DAF ice sheet and that the northernmost ridges may have formed closer to a stable former ice margin, supported by their proximity to a putative proglacial paleolake in Argentea Planum (Head and Pratt, 2001). Ridge B is similar in length to the >300 km-long type 1 (Brennand, 2000) "Haricana interlobate moraine", or "Abitibi esker", in Quebec (Brennand and Shaw, 1996). Although Ridge B does not terminate in the region of the

putative paleolake (Head and Pratt, 2001), ponding of meltwater in the basin of East Argentea Planum where it does terminate, is viable. A valley at the distal end of East Argentea Planum may provide evidence for drainage of large volumes of water from this basin, although the existence of this valley-feature is contested (Tanaka and Kolb, 2001; Head and Pratt, 2001; Ghatan and Head, 2004; Fastook et al., 2012; Tanaka et al., 2014a). Meltwater discharges of the order of 10^3-10^5 m^3s^{-1} reconstructed from ridge geometry by Scanlon and Head (2015) are within the range observed for ice sheet flood discharges on Earth (Lewis et al., 2006) and, if sustained, could allow channel persistence even in the absence of a proglacial water body. Stagnation of the overlying ice and mass-loss by subsequent downwasting, as suggested by previous workers who interpret the Dorsa Argentea as eskers (Metzger, 1991; Head and Pratt, 2001; Scanlon and Head, 2015), could provide a further explanation for stability of long esker-forming R-channels (Brennand, 2000). Emergence of very well-preserved eskers from stagnant, downwasting ice has been observed at Malaspina Glacier in Alaska (Gustavson and Boothroyd, 1987).

However, despite detailed investigations of the geomorphology and sedimentology of terrestrial eskers (e.g., Brennand, 1994; Brennand and Shaw, 1996; Brennand, 2000; Mäkinen, 2003), great uncertainty remains over the nature of sedimentation of long terrestrial eskers. The present inability to investigate the internal structure of the Dorsa Argentea means that we cannot conclude with certainty that, if the Dorsa Argentea are eskers, they formed either by synchronous or time-transgressive deposition. However, the evidence obtained in this and previous studies of the Dorsa Argentea suggests synchronous deposition may be more likely.

Shorter ridge segments between and adjacent to longer, often braided or branching ridges (Fig. 5) of the Dorsa Argentea could be remnants of shorter drainage pathways from which water was scavenged along hydraulic potential gradients towards longer, lower-pressure conduits nearby during development of the drainage network (Shreve, 1972; Storrar et al., 2014a). Testing of the hypothesis proposed by Kress and Head (2015) that this

adjacent network was akin to distributed glacier drainage systems on Earth is beyond the scope of the present study, considering the lack of terrestrial analogues of ridges of sediment formed in such systems.

6.2 Cross-sectional dimensions and crest morphology

The significant difference in height between sharp-crested (mean = 46 m; S.E. = 2 m) and broad-crested (mean = 30 m; S.E. = 3 m) sections of the Dorsa Argentea indicates that variation in crest morphology along ridge profiles likely reflects original features of the ridges. Post-depositional erosion, which on Earth causes rounding of terrestrial inverted channels and can result in similar morphology to terrestrial eskers (Burr et al., 2009) may only account for ~<1 m of the observed height difference between broad- and sharp-crested sections of the Dorsa Argentea, given typical rates of erosion that have prevailed since the time of their formation (Carr and Head, 2010). Lower aspect ratios of sharp- relative to broad-crested sections are largely an outcome of differences in ridge height. According to Shreve's (1985a) theory of esker formation, greater sensitivity of roofs of subglacial conduits to changes in the energy available for melt leads to higher rates of melting and freezing than at the conduit walls. This differential sensitivity to melt may explain the differences in aspect ratio between sections of the Dorsa Argentea with sharp and broad crest morphologies.

6.3 Topographic Relationships

Melt regimes in terrestrial subglacial conduits are predicted to change to regimes of wall freezing on bed slopes ~1.7 times the ice surface slope (Shreve, 1972, 1985a). Under an ice surface slope of ~0.06 ° reconstructed by Scanlon and Head (2015) for the Dorsa Argentea, this transition would be expected to occur on bed slopes of ~0.01°, assuming this relationship holds on Mars. Statistically insignificant t-values for the constants of the regression models (Table 6) confirm that the transition between increases and decreases in height occurs on approximately level bed slopes around the origin of the scatterplots in Fig. 12. Such a low critical threshold of transition between melting and freezing regimes could explain the low proportion of CS profiles with multiple-crested CS morphologies (<1 %).

51

Reduction to near-negligible height of Ridge A as it traverses the crest of a degraded crater rim (Fig. 13b) may be explained by a combination of weakening of conduit roof melting, and increases in sediment transport capacity in an esker-forming conduit at the crest of the crater rim due to depression of contours of hydraulic equipotential (Fig. 2) (Shreve, 1972, 1985a).

The lack of discernible difference in bed slopes occupied by sharp and broad crest types may be an outcome of gradual (as opposed to immediate) transitions between crest morphological types when bed slope reaches the critical slope for morphological transition of the ridge crest under the esker hypothesis. Given the low topographic slopes over which the Dorsa Argentea pass, and the significant difference in height between ridge sections with sharp and broad crest morphologies, this explanation is not inconceivable. However, alteration of ridge dimensions (and potentially morphology) by a mantle which drapes certain ridge sections (excluded from the present study) upon which Head and Hallet (2001a) based their assertion of a relationship between bed topography and ridge crest morphology (Fig. 6c), highlights the requirement for further tests for this relationship.

Further assessment of the processes responsible for formation of different crest morphologies along the ridges may be possible with improvements in the coverage of high-resolution (~0.3-1.25 m/pixel) images and High-resolution Imaging Science Experiment (HiRISE) or CTX DEM products. Strong stratification of sediments in terrestrial eskers with sharp crest morphologies contrasts with well sorted, massive deposits typical of broad-crested sections. This has been related to changes in deposition conditions in response to topography (Shreve, 1972, 1985a; Brennand, 2000). Well-developed kilometre-scale layering structures in the sloping sides of Ridge B therefore provide potential for tests for differences in formation conditions between sharp-crested and broad-crested sections of the Dorsa Argentea in future assessment of the esker hypothesis.

6.4. Lateral Pedestal Feature

The lateral pedestal feature identified on the outer bend of a section of Ridge B (Fig. 14.) may be considered as evidence to support the alternative hypothesis that the Dorsa Argentea are inverted channels (Tanaka and Kolb, 2001; Tanaka et al., 2014b).

Inverted channels are ridges formed by differential erosion between resistant deposits infilling fluvial channels and more erodible material in the surrounding region. Resistant channel infill may consist of chemically cemented sediments, coarse-grained fluvial lag deposits or lava flows (Williams et al., 2007; Burr et al., 2009). Terrestrial inverted channels such as those in Utah, USA (Williams et al., 2007) have diverse crest morphologies, ranging from flat-topped plateaus with steep side escarpments, to multilevel ridge configurations where the inverted channel sits atop a broader exhumed pedestal ridge (Burr et al., 2009, Fig. 13). In inverted fluvial systems, such pedestals may form as an outcome of a differential in resistance to erosion between channel infill and finer overbank deposits. The interpretation of the Dorsa Argentea as inverted channels (Tanaka and Kolb, 2001; Tanaka et al., 2014b), which is a modification of the lava-flow hypothesis of Tanaka and Scott (1987) is based upon interpretation of lobate fronts at the margins of the DAF as evidence of its formation by flows of fluidised regolith. Flows could have been mobilised by expulsion of subsurface accumulations of water and CO_2, triggered by impact events, or seismic or intrusive magmatic activity (Tanaka and Kolb, 2001; Ghatan and Head, 2004) during the Hesperian period, which was characterised by extensive resurfacing by volcanic activity (Carr and Head, 2010; Tanaka et al., 2014b). The shield and cone structures of the Hesperian polar edifice unit, which exists in several outcrops within the DAF, (Fig. 1) (Tanaka et al., 2014a) may represent vent sources for this cryovolcanic material (Tanaka and Kolb, 2001; Ghatan and Head, 2004; Tanaka et al., 2014b).

Tanaka and Kolb (2001) suggest that the Dorsa Argentea formed as *'…smaller eruptions of volatile-rich material … resulted in narrow, sinuous channel deposits within aggrading fine-grained unconsolidated material perhaps produced by gaseous discharge of subsurface volatiles'* (Tanaka and Kolb, 2001, p. 3) which subsequently underwent erosion

at a greater rate than the more resistant channel infill, leading to inversion of the channel topography. Tanaka and Kolb's (2001) study employs images from the Mars Orbiter Camera at ~1.5-12m/pixel., which is the highest resolution dataset used to date in analysis of the Dorsa Argentea.

Distinction between the inverted channel and glacial esker hypotheses for the origin of the Dorsa Argentea is limited by the fact that, over time, erosional rounding of the ridge form (Williams et al., 2007) introduces difficulties in distinguishing between inverted fluvial channels and eskers on the basis of visual assessment alone (Burr et al., 2009). However, when considered alongside previous studies that weaken the inverted channel hypothesis (e.g., Howard, 1981; Ruff and Greeley, 1990; Head, 2000a; Head and Pratt, 2001) we argue that the rigorous statistical testing of planar geometry, morphology and topographic relationships for the Dorsa Argentea presented in the present study strengthens the hypothesis that the Dorsa Argentea are eskers. Therefore, it is proposed that the lateral pedestal feature identified on Ridge B (Fig. 14) may be analogous to lateral fans occurring predominantly on the outer bends of eskers in south-central Ontario (Brennand, 1994). As the major ridge passing into East Argentea Planum (Fig. 5), Ridge B may represent the main drainage pathway funnelling meltwater from the Argentea Planum catchment of a former DAF ice sheet. Intrusion of water into cavities in the surrounding basal ice as water pressure exceeded ice overburden under high discharges (Brennand, 1994) on this major drainage pathway is tentatively proposed as an explanation for the pedestal. HiRISE data would allow assessment of the sedimentary properties and stratigraphic relationships of this pedestal feature in order to further test this hypothesis.

6.5 Implications

A growing body of literature uses the esker interpretation as a basis for inferences about the character of a putative former ice sheet thought to have extended into the region of the Dorsa Argentea during Mars' Hesperian period (~2.7-~3.55 Ga), despite a lack of detailed quantitative comparison with a large sample of terrestrial eskers or rigorous

statistical tests for esker-like topographic relationships (e.g., Howard, 1981; Kargel and Strom, 1992; Kargel, 1993; Head, 2000a, 2000b; Head and Pratt, 2001; Ghatan and Head, 2004; Scanlon and Head, 2015; Kress and Head, 2015). The more rigorous quantitative and statistical analysis of the Dorsa Argentea presented here, and comparison with a large sample of terrestrial eskers, improves confidence that the Dorsa Argentea are eskers formed by deposition of sediment in subglacial meltwater conduits. In the present day, as throughout most of the present Amazonian period on Mars, mean annual south polar surface temperatures of -100°C preclude basal melting of the cold-based polar ice deposits that remain (Fastook et al., 2012). Evidence for drainage beneath a former ice sheet therefore provides insight into the history of glaciation and its response to climate changes on Mars, thought to be associated with variations in planetary obliquity (Souness and Hubbard, 2012). The implications of evidence for a formerly more extensive south polar ice sheet for past environmental changes on Mars are discussed in detail by Head and Pratt (2001), Fastook et al. (2012), Scanlon and Head (2015) and Kress and Head (2015). The new quantitative characterisations of the Dorsa Argentea contained within this study may provide useful constraints for parameters in modelling studies of this putative former ice sheet, its hydrology, and mechanisms that drove its eventual retreat.

Subglacial meltwater production supports the potential for former habitability of glacial environments on Mars. Glaciofluvial deposits may represent ancient fossilization environments, providing a focus for targeted exploration for evidence of life on Mars (Head and Pratt, 2001).

7. Conclusion

This study supports the hypothesis that the Dorsa Argentea are eskers formed by deposition in subglacial meltwater channels beneath a former DAF ice sheet.

Statistical distributions of lengths and sinuosities of the Dorsa Argentea are similar to those recently quantified by Storrar et al. (2014a) for terrestrial eskers formed during

deglaciation of the Laurentide Ice Sheet. Small deviations in the similarities for the two populations may be (at least partially) accounted for by differences in their degree of fragmentation arising from different regimes of erosion between Earth and Mars. Low levels of fragmentation and higher ridge sinuosity of the northernmost ridges in the DAF may support synchronous formation of the ridges in subglacial conduits extending towards the interior of an ice sheet that thinned towards its northern margin, perhaps terminating in a proglacial lake. This contrasts with the time-transgressive mode of formation proposed by Storrar et al. (2014a) for the Canadian eskers. However, debate over time-transgressive and synchronous deposition mechanisms for the formation of terrestrial eskers is ongoing and detailed sedimentological analyses of internal structure of the ridges would be required to corroborate arguments in support of either of these mechanisms for formation of the Dorsa Argentea.

Significant differences in cross-sectional dimensions of ridge sections with sharp and broad crest morphologies provide support for differences in conditions of formation along the lengths of individual ridges. Rigorous quantitative tests of previously observed relationships between ridge height and longitudinal bed slope, similar to those explained by the physics of meltwater flow through subglacial meltwater conduits for terrestrial eskers (Shreve, 1972, 1985b; Head and Hallet, 2001a), confirm the statistical significance of these relationships for three of four major Dorsa Argentea ridges.

The new quantitative characterisations of the Dorsa Argentea contained within this study may provide useful constraints for parameters in modelling studies of this putative former ice sheet, its hydrology, and mechanisms that drove its eventual retreat.

8. Acknowledgements

References

Anderson, R.S., Anderson, S.P., 2010. Geomorphology: the mechanics and chemistry of landscapes. Cambridge University Press, Cambridge.

Banerjee, I., McDonald, B.C., 1975. Nature of Esker Sedimentation. Glacifluvial Glacilacustrine Sediment. Soc. Econ. Paleontol. Mineral. Spec. Publ. 23, 304–320.

Banks, M.E., Lang, N.P., Kargel, J.S., McEwen, A.S., Baker, V.R., Grant, J.A., Pelletier, J.D., Strom, R.G., 2009. An analysis of sinuous ridges in the southern Argyre Planitia, Mars using HiRISE and CTX images and MOLA data. J. Geophys. Res. Planets 114, E09003. doi:10.1029/2008JE003244

Benn, D.I., Evans, D.J.A., 2010. Glaciers & Glaciation, Second. ed. Hodder Education, London.

Bernhardt, H., Hiesinger, H., Reiss, D., Ivanov, M., Erkeling, G., 2013. Putative eskers and new insights into glacio-fluvial depositional settings in southern Argyre Planitia, Mars. Planet. Space Sci. 85, 261–278. doi:10.1016/j.pss.2013.06.022

Brennand, T.A., 2000. Deglacial meltwater drainage and glaciodynamics: inferences from Laurentide eskers, Canada. Geomorphology 32, 263–293. doi:10.1016/S0169-555X(99)00100-2

Brennand, T.A., 1994. Macroforms, large bedforms and rhythmic sedimentary sequences in subglacial eskers, south-central Ontario: implications for esker genesis and meltwater regime. Sediment. Geol. 91, 9–55. doi:10.1016/0037-0738(94)90122-8

Brennand, T.A., Shaw, J., 1996. The Harricana glaciofluvial complex, Abitibi region, Quebec: its genesis and implications for meltwater regime and ice-sheet dynamics. Sediment. Geol. 102, 221–262. doi:10.1016/0037-0738(95)00069-0

Burr, D.M., Enga, M.-T., Williams, R.M.E., Zimbelman, J.R., Howard, A.D., Brennand, T.A., 2009. Pervasive aqueous paleoflow features in the Aeolis/Zephyria Plana region, Mars. Icarus 200, 52–76. doi:10.1016/j.icarus.2008.10.014

Carr, M.H., Head, J.W., III 2010. Geologic history of Mars. Earth Planet. Sci. Lett., Mars Express after 6 Years in Orbit: Mars Geology from Three-Dimensional Mapping by the High Resolution Stereo Camera (HRSC) Experiment 294, 185–203. doi:10.1016/j.epsl.2009.06.042

Clark, P.U., Walder, J.S., 1994. Subglacial drainage, eskers, and deforming beds beneath the Laurentide and Eurasian ice sheets. Geol. Soc. Am. Bull. 106, 304–314.

Erkeling, G., Reiss, D., Hiesinger, H., Ivanov, M.A., Hauber, E., Bernhardt, H., 2014. Landscape formation at the Deuteronilus contact in southern Isidis Planitia, Mars: Implications for an Isidis Sea? Icarus 242, 329–351. doi:10.1016/j.icarus.2014.08.015

Fastook, J.L., Head, J.W., Marchant, D.R., Forget, F., Madeleine, J.-B., 2012. Early Mars climate near the Noachian–Hesperian boundary: Independent evidence for cold conditions from basal melting of the south polar ice sheet (Dorsa Argentea Formation) and implications for valley network formation. Icarus 219, 25–40. doi:10.1016/j.icarus.2012.02.013

Flowers, G.E., 2015. Modelling water flow under glaciers and ice sheets. Proc. R. Soc. Math. Phys. Eng. Sci. 471, 20140907. doi:10.1098/rspa.2014.0907

Fountain, A.G., Walder, J.S., 1998. Water flow through temperate glaciers. Rev. Geophys. 36, 299–328. doi:10.1029/97RG03579

Gallagher, C., Balme, M., 2015. Eskers in a complete, wet-based glacial system in the Phlegra Montes region, Mars. Earth Planet. Sci. Lett. 431, 96–109. doi:10.1016/j.epsl.2015.09.023

Ghatan, G.J., Head, J.W., III, 2004. Regional drainage of meltwater beneath a Hesperian-aged south circumpolar ice sheet on Mars. J. Geophys. Res. 109. doi:10.1029/2003JE002196

Gustavson, T.C., Boothroyd, J.C., 1987. A depositional model for outwash, sediment sources, and hydrologic characteristics, Malaspina Glacier, Alaska: A modern analog of the southeastern margin of the Laurentide Ice Sheet. Geol. Soc. Am. Bull. 99, 187–200. doi:10.1130/0016-7606(1987)99<187:ADMFOS>2.0.CO;2

Hartmann, W.K., 2005. Martian cratering 8: Isochron refinement and the chronology of Mars. Icarus, Mars Polar Science III 174, 294–320. doi:10.1016/j.icarus.2004.11.023

Head, J.W., III, 2000a. Tests for Ancient Polar Deposits on Mars: Origin of Esker-like Sinuous Ridges (Dorsa Argentea) Using MOLA Data. Lunar Planet. Sci. Conf. XXXI Abstract #1116.

Head, J.W., III, 2000b. Tests for Ancient Polar Deposits on Mars: Morphology and Topographic Relationships of Esker-like Sinuous Ridges (Dorsa Argentea) Using MOLA Data. Lunar Planet. Sci. Conf. XXXI Abstract #1117.

Head, J.W., III, Hallet, B., 2001a. Origin of Sinuous Ridges in the Dorsa Argentea Formation: New Observations and Tests of the Esker Hypothesis. Lunar Planet. Sci. Conf. XXXII Abstract #1373.

Head, J.W., III, Hallet, B., 2001b. Origin of Sinuous Ridges in the Dorsa Argentea Formation: Additional Criteria for Tests of the Esker Hypothesis. Lunar Planet. Sci. Conf. XXXII Abstract #1366.

Head, J.W., Pratt, S., 2001. Extensive Hesperian-aged south polar ice sheet on Mars: Evidence for massive melting and retreat, and lateral flow and ponding of meltwater. J. Geophys. Res. Planets 106, 12275–12299. doi:10.1029/2000JE001359

Hooke, R., LeB, Fastook, J., 2007. Thermal conditions at the bed of the Laurentide ice sheet in Maine during deglaciation: implications for esker formation. J. Glaciol. 53, 646–658. doi:10.3189/002214307784409243

Howard, A.D., 1981. Etched plains and braided ridges of the south polar region of Mars: Features produced by basal melting of ground ice? Rep. Planet. Geol. Program 1981 Natl. Aeronaut. Space Adm. Tech. Memo. 84211, 286–288.

Hubbard, B., Nienow, P., 1997. Alpine subglacial hydrology. Quat. Sci. Rev. 16, 939–955. doi:10.1016/S0277-3791(97)00031-0

Ivanov, M.A., Hiesinger, H., Erkeling, G., Hielscher, F.J., Reiss, D., 2012. Major episodes of geologic history of Isidis Planitia on Mars. Icarus 218, 24–46. doi:10.1016/j.icarus.2011.11.029

Jaumann, R., Neukum, G., Behnke, T., Duxbury, T.C., Eichentopf, K., Flohrer, J., Gasselt, S. v., Giese, B., Gwinner, K., Hauber, E., Hoffmann, H., Hoffmeister, A., Köhler, U., Matz, K.-D., McCord, T.B., Mertens, V., Oberst, J., Pischel, R., Reiss, D., Ress, E., Roatsch, T., Saiger, P., Scholten, F., Schwarz, G., Stephan, K., Wählisch, M., 2007. The high-resolution stereo camera (HRSC) experiment on Mars Express: Instrument aspects and experiment conduct from interplanetary cruise through the nominal mission. Planet. Space Sci. 55, 928–952. doi:10.1016/j.pss.2006.12.003

Kamb, B., 1987. Glacier surge mechanism based on linked cavity configuration of the basal water conduit system. J. Geophys. Res. Solid Earth 92, 9083–9100. doi:10.1029/JB092iB09p09083

Kargel, J.S., 1993. Geomorphic processes in the Argyre-Dorsa Argentea region of Mars. Lunar Planet. Sci. Conf. XXIV Abstract #1378.

Kargel, J.S., Strom, R.G., 1992. Ancient glaciation on Mars. Geology 20, 3–7. doi:10.1130/0091-7613(1992)020<0003:AGOM>2.3.CO;2

Kress, A.M., Head, J.W., 2015. Late Noachian and early Hesperian ridge systems in the south circumpolar Dorsa Argentea Formation, Mars: Evidence for two stages of melting of an extensive late Noachian ice sheet. Planet. Space Sci. 109–110, 1–20. doi:10.1016/j.pss.2014.11.025

Lewis, A.R., Marchant, D.R., Kowalewski, D.E., Baldwin, S.L., Webb, L.E., 2006. The age and origin of the Labyrinth, western Dry Valleys, Antarctica: Evidence for extensive middle Miocene subglacial floods and freshwater discharge to the Southern Ocean. Geology 34, 513–516. doi:10.1130/G22145.1

Mäkinen, J., 2003. Time-transgressive deposits of repeated depositional sequences within interlobate glaciofluvial (esker) sediments in Köyliö, SW Finland. Sedimentology 50, 327–360. doi:10.1046/j.1365-3091.2003.00557.x

Malin, M.C., Bell, J.F., Cantor, B.A., Caplinger, M.A., Calvin, W.M., Clancy, R.T., Edgett, K.S., Edwards, L., Haberle, R.M., James, P.B., Lee, S.W., Ravine, M.A., Thomas, P.C., Wolff, M.J., 2007. Context Camera Investigation on board the Mars Reconnaissance Orbiter. J. Geophys. Res. 112. doi:10.1029/2006JE002808

Mangold, N., 2000. Giant Paleo-eskers of Mauritania: Analogs for Martian Esker-Like Landforms. Second Int. Conf. Mars Polar Sci. Explor. Abstract #4031.

Metzger, S.M., 1992. The Eskers of New York State: Formation Process Implications and Esker-like Features on the Planet Mars. Lunar Planet. Sci. Conf. XXIII Abstract #1448.

Metzger, S.M., 1991. A survey of esker morphometries, the connection to New York state glaciation and criteria for subglacial melt-water channel deposits on the planet Mars. Lunar Planet. Sci. Conf. XXII Abstract #1444.

Milkovich, S.M., Head, J.W., Pratt, S., 2002. Meltback of Hesperian-aged ice-rich deposits near the south pole of Mars: Evidence for drainage channels and lakes. J. Geophys. Res. Planets 107, 10–1. doi:10.1029/2001JE001802

Neukum, G., Jaumann, R., the HRSC Co-Investigator and Experiment Team, 2004. HRSC: The high resolution stereo camera of Mars Express, in: Wilson, A. (Ed.), Mars Express: The Scientific Payload, European Space Agency Special Publication 1240. pp. 17–35.

Parker, T.J., Pieri, D.C., Saunders, R.S., 1986. Morphology and distribution of sinuous ridges in central and southern Argyre. Natl. Aeronaut. Space Adm. Tech. Memo. 88383, 468–470.

Perkins, A.J., Brennand, T.A., Burke, M.J., 2016. Towards a morphogenetic classification of eskers: Implications for modelling ice sheet hydrology. Quat. Sci. Rev. 134, 19–38. doi:10.1016/j.quascirev.2015.12.015

Phillips, R.J., Davis, B.J., Tanaka, K.L., Byrne, S., Mellon, M.T., Putzig, N.E., Haberle, R.M., Kahre, M.A., Campbell, B.A., Carter, L.M., Smith, I.B., Holt, J.W., Smrekar, S.E., Nunes, D.C., Plaut, J.J., Egan, A.F., Titus, T.N., Seu, R., 2011. Massive CO2 Ice Deposits Sequestered in the South Polar Layered Deposits of Mars. Science 332, 838–841. doi:10.1126/science.1203091

Punkari, M., 1997. Glacial and glaciofluvial deposits in the interlobate areas of the Scandinavian ice sheet. Quat. Sci. Rev., Ice-Contact Sedimentation: Processes and Deposits 16, 741–753. doi:10.1016/S0277-3791(97)00020-6

Röthlisberger, H., 1972. Water pressure in intra- and subglacial channels. J. Glaciol. 11, 117–203.

Ruff, S.W., Greeley, R., 1990. Sinuous Ridges of the South Polar Region, Mars: Possible Origins. Lunar Planet. Sci. Conf. XXI Abstract #1532.

Scanlon, K.E., Head, J.W., 2015. The recession of the Dorsa Argentea Formation ice sheet: geologic evidence and climate simulations. Lunar Planet. Sci. Conf. XLVI Abstract #2247.

Shreve, R.L., 1985a. Esker characteristics in terms of glacier physics, Katahdin esker system, Maine. Geol. Soc. Am. Bull. 96, 639. doi:10.1130/0016-7606(1985)96<639:ECITOG>2.0.CO;2

Shreve, R.L., 1985b. Late Wisconsin ice-surface profile calculated from esker paths and types, Katahdin esker system, maine. Quat. Res. 23, 27–37. doi:10.1016/0033-5894(85)90069-9

Shreve, R.L., 1972. Movement of water in glaciers. J. Glaciol. 11, 205–214.

Som, 2008. The Mars Orbiter Laser Altimeter dataset: Limitations and improvements. Mars J. 4, 14–26. doi:10.1555/mars.2008.0002

Souness, C., Hubbard, B., 2012. Mid-latitude glaciation on Mars. Prog. Phys. Geogr. 36, 238–261. doi:10.1177/0309133312436570

Storrar, R.D., Evans, D.J.A., Stokes, C.R., Ewertowski, M., 2015. Controls on the location, morphology and evolution of complex esker systems at decadal timescales, Breiðamerkurjökull, southeast Iceland. Earth Surf. Process. Landf. 40, 1421–1438. doi:10.1002/esp.3725

Storrar, R.D., Stokes, C.R., Evans, D.J.A., 2014a. Morphometry and pattern of a large sample (>20,000) of Canadian eskers and implications for subglacial drainage beneath ice sheets. Quat. Sci. Rev. 105, 1–25. doi:10.1016/j.quascirev.2014.09.013

Storrar, R.D., Stokes, C.R., Evans, D.J.A., 2014b. Increased channelization of subglacial drainage during deglaciation of the Laurentide Ice Sheet. Geology 42, 239–242. doi:10.1130/G35092.1

Storrar, R.D., Stokes, C.R., Evans, D.J.A., 2013. A map of large Canadian eskers from Landsat satellite imagery. J. Maps 9, 456–473. doi:10.1080/17445647.2013.815591

Tanaka, K.L., Kolb, E.J., 2001. Geologic History of the Polar Regions of Mars Based on Mars Global Surveyor Data I. Noachian and Hesperian Periods. Icarus 154, 3–21. doi:10.1006/icar.2001.6675

Tanaka, K.L., Scott, D.H., 1987. Geologic map of the polar regions of Mars. U.S Geological Survey Miscellaneous Investigations Series Map 1-1802-C.

Tanaka, K.L., Skinner, J.A., Dohm, J.M., Irwin III, R.P., Kolb, E.J., Fortezzo, C.M., Platz, T., Michael, G.G., Hare, T., 2014a. Geologic Map of Mars. USGS Scientific Investigations Map 3292.

Tanaka, K.L., Skinner, J.A., Dohm, J.M., Irwin III, R.P., Kolb, E.J., Fortezzo, C.M., Platz, T., Michael, G.G., Hare, T., 2014b. Geologic map of Mars, Pamphlet to accompany Scientific Investigations Map 3292. US Geological Survey.

Williams, R.M., Chidsey Jr, T.C., Eby, D.E., 2007. Exhumed paleochannels in central Utah—Analogs for raised curvilinear features on Mars, in: Hylland, M.D., Clark, D.L., Chidsey, T.C. (Eds.), Central Utah - Diverse Geology of a Dynamic Landscape, Utah Geological Association Publication.

Zuber, M.T., Smith, D.E., Solomon, S.C., Muhleman, D.O., Head, J.W., Garvin, J.B., Abshire, J.B., Bufton, J.L., 1992. The Mars Observer Laser Altimeter Investigation. J. Geophys. Res. 97, 7781–7797.